THEORETICAL STUDIES OF DYE-LABELED DNA SYSTEMS WITH APPLICATIONS TO FLUORESCENCE RESONANCE ENERGY TRANSFER

By
ELENA DOLGHIH

A DISSERTATION PRESENTED TO THE GRADUATE SCHOOL
OF THE UNIVERSITY OF FLORIDA IN PARTIAL FULFILLMENT
OF THE REQUIREMENTS FOR THE DEGREE OF
DOCTOR OF PHILOSOPHY

UNIVERSITY OF FLORIDA

2009

To mom and dad, Valentina and Nikolai Dolghih, and to my sister, Leiza

ACKNOWLEDGMENTS

I would like to thank first and foremost my two main advisors, Jeffrey Krause and Adrian Roitberg for their guidance and support throughout my studies. I owe special gratitude to Dr. Roitberg for taking me under his wing and providing much needed advice as well as inspiration in the past couple of years.

I would also like to thank my supervisory committee, Dr. So Hirata, Dr. Hai-Ping Cheng, and Dr. Stephen Hagen. Special thanks go to my collaborators, Dr. Marcia Levitus, Dr. Fernando Noriega, Dr. Adrian Turjanski and Dr. Brent Krueger as well as to their students for providing experimental data and insight that made my theoretical studies so much more interesting.

Lastly, I would like to thank my family, my mom and dad, Валентина and Николай Долгих and my sister, Лиза. I could not wish for more supportive family and am very grateful for all the advice and encouragement they provided over the years. Without them none of this could have been possible.

TABLE OF CONTENTS

page

LIST OF TABLES

LIST OF FIGURES

Abstract of Dissertation Presented to the Graduate School
of the University of Florida in Partial Fulfillment of the
Requirements for the Degree of Doctor of Philosophy

THEORETICAL STUDIES OF DYE-LABELED DNA SYSTEMS WITH APPLICATIONS TO FLUORESCENCE RESONANCE ENERGY TRANSFER By

Elena Dolghih

May 2009

Chairs: Jeffrey L. Krause, Adrian E. Roitberg
Major: Chemistry

The complex and indispensable role that nucleic acids play in the existence of all living organisms has made them subject of many interesting studies over the decades. One of the most popular techniques used to examine interactions of these molecules with their environment, each other, and proteins is single-molecule Fluorescence Resonance Energy Transfer (smFRET). The process of resonance energy transfer is based on the ability of an electronically excited fluorescent molecule (the donor) to transfer energy through space to a second molecule (acceptor) with an efficiency that is defined by Förster theory to depend on the donor-acceptor distance raised to the negative power of six. In FRET experiments, measured efficiency is used to infer interdye distance and, hence, dynamic and structural changes in a system. Thus, FRET has been used to investigate, among other processes, conformational dynamics of Holliday junctions, folding states of ribozyme hairpin, DNA melting, and DNA-cofactor interactions in which relative distance changes were correlated to interconversion between various states of the systems. Measuring relative rather than absolute distances remains a standard approach in FRET experiments even at a single-molecule level due to lack of knowledge about the probe position and orientation with respect to each other and the system. The long linkers through which the dyes are attached to DNA, the large size of the probes themselves, as well as the possibility of their interaction with the system add to this uncertainty.

In this work we describe a molecular dynamics study of several dye-DNA systems in which we examine how fluorescent probes interact with DNA and the effects of these interactions on FRET. Structural fluctuations in interchromophore distances and dipole orientations of the probes, as well as rates and efficiencies of energy transfer are evaluated carefully in the light of Förster-proposed approximations. Theoretical results are compared to available experimental data and possible improvements in system design with respect to the location and the mode of attachment of the probes are proposed.

CHAPTER 1
INTRODUCTION

1.1 Absorption and Emission of Light

Within many modern biological sciences including molecular biology, biochemistry, biophysics, and nanobiology, fluorescence techniques are used on a daily basis to probe fundamental questions about how molecules interact with each other and their environment. Among the processes studied are protein and DNA folding, replication, translation, catalysis, enzymatic mechanisms, signal transduction, and many others. At the basis of these studies lies the phenomenon of fluorescence – a radiative emission of photons from molecular excited states. This process is one of several by which an excited molecule can return to the ground state.[1]

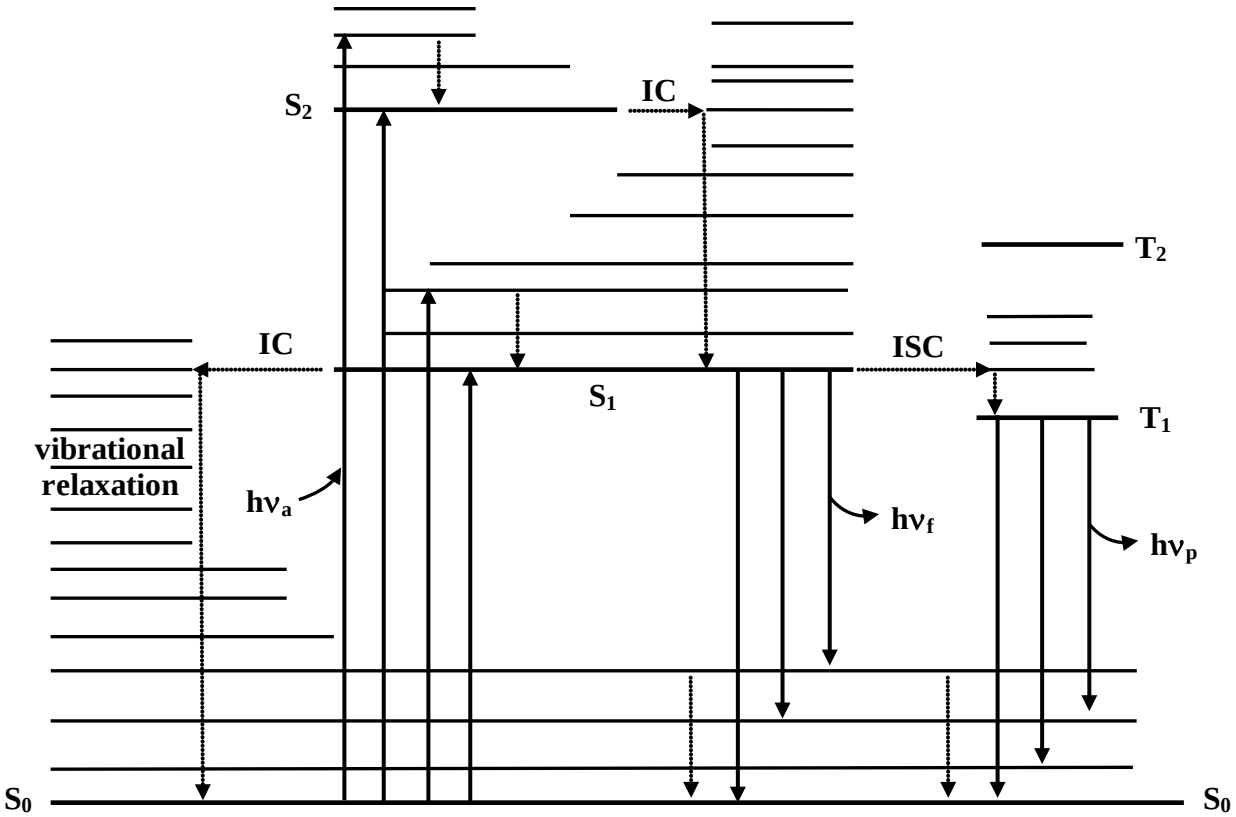

Figure 1-1. A diagram of various emission pathways of an excited molecule. S_0 is the singlet ground state. S_1 and S_2 are first and second singlet electronic states and T_1 and T_2 are corresponding triplet states. Absorbed photons are represented by $h\nu_a$. Emitted photons are $h\nu_f$ and $h\nu_p$ for fluorescence and phosphorescence, respectively. IC is internal conversion and ISC is intersystem crossing.

As illustrated in the diagram, after instantaneous light absorption (Frank-Condon principle) and internal relaxation back to the lowest level of excitation (S_1) through internal conversion and vibrational relaxation, deexcitation of the molecule can happen through three general pathways: radiative decay (fluorescence), nonradiative decay (often due to quenching or solvent relaxation) and phosphorescence, which involves a singlet-to-triplet transition (intersystem crossing) and is not very common. All of these processes are affected to various degrees by the local environment surrounding the excited molecule. The relatively simple setup required for fluorescence measurements and the sensitivity of the fluorescent emission to the orientation and location of the molecule and environmental factors makes fluorescent techniques extremely appealing and widely used.[2]

Not the least of this appeal lies in the technology developed recently that enables study of single-molecule systems, rather than ensembles of molecules.[3-7] The wealth of information uncovered by such measurements includes details about the real-time dynamics and complete structural distribution of a system. Various states and intermediates of a system, which would have previously been hidden due to ensemble averaging, as well as reaction rates and conformational fluctuations of the molecule, can now be detected easily, quantified and analyzed.[8-11]

1.2 Nucleic Acids

Nucleic acids (NA) form one of the four major classes of biological molecules and are responsible for storage and transfer of genetic information within living organisms. The two types of NA - deoxyribonucleic acid (DNA) and ribonucleic acid (RNA) - are biopolymers that consist of repeating units called nucleotides. Each nucleotide includes a base, a 5-carbons sugar (deoxyribose or ribose for DNA and RNA, respectively) and a phosphate. There are four different types of bases in DNA: adenine, thymine, cytosine, and guanine (Figure 1-2), whereas

in RNA thymine is replaced with uracil. While RNA is usually single-stranded, DNA is composed of two nucleotide polymers that form a double-helix structure held together by hydrogen bonding between adenine-thymine and guanine-cytosine pairs. The two strands twist to form a helix in a way that results in two grooves of different widths known as major and minor grooves. B-DNA, the most common form of DNA, has 10 base pairs per turn, 36° twist and 3.4 Å rise per base pair.[12]

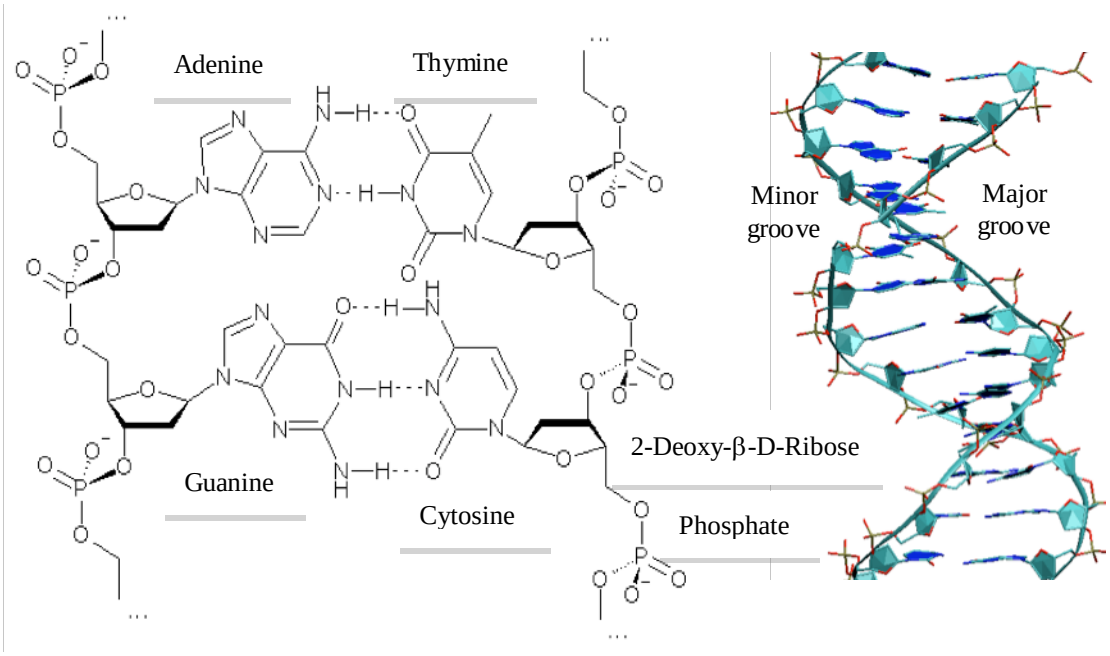

Figure 1-2. Nucleic acid structure.

1.3 Förster Theory

Among the many available single-molecule fluorescence techniques, single-molecule resonance energy transfer (smFRET) is one of the most popular and widely used. It is based on the phenomenon of resonance energy transfer, observed for the first time by Perrin in the 1930s[13] and described formally by Förster in the 1940s.[14-16] The process is based on the ability of an electronically excited molecule (the donor, D) to transfer energy through space to a second molecule (the acceptor, A). It is been used by structural biologists through FRET experiments, which are known by a variety of names[17], since its effectiveness was demonstrated in the 1960s

and 1970s by the Stryer group and others.[18-23] Chromophores of various types are attached to systems ranging from peptides and oligonucleotides to proteins, nucleic acids and membranes. Fluorescence data are used to infer distances, and hence structure, as well as relative distances and dynamic structural data.[4, 24-28] This is particularly important for biological systems in solution, for which direct structural information is difficult to obtain. In particular, the last 5-10 years have seen a dramatic increase in the use of FRET as a number of laboratories have applied it to single molecules.[24, 27, 29-34]

At the basis of most analyses of FRET experiments is the familiar form of the Förster equation[16],

$$k_{RET} = \frac{9000(\ln 10)\kappa^2 Q_D J(\lambda)}{128\pi^5 \tau_D N_A \eta^4} = \frac{1}{\tau_D}\left(\frac{R_0}{R}\right)^6 \qquad (1\text{-}1)$$

in which k_{RET} is the rate constant of resonance energy transfer in inverse time units, κ^2 is an orientation factor between the donor and acceptor transition dipoles, Q_D is the quantum yield of the donor in the absence of the acceptor, τ_D is the lifetime of the donor in the absence of the acceptor in time units, $J(\lambda)$ is the spectral overlap of the emission spectrum of the donor with the absorption spectrum of the acceptor in units of M^{-1} cm^3, η is the index of refraction of the medium, N_A is Avogadro's number in mol^{-1}, R is the distance between the centers of the donor and the acceptor transition dipoles in cm and R_0, the Förster radius, is the distance at which the efficiency is 50% and is also in centimeters. The spectral overlap is computed as following,

$$J(\lambda) = \int f_D(\lambda)\varepsilon_A(\lambda)\lambda^4 d\lambda \qquad (1\text{-}2)$$

where f_D is the normalized donor emission spectrum and ε_A is the acceptor molar extinction coefficient (Figure 1-3A). The orientation factor is defined on the basis of the orientation of the transition dipoles of the probes and can be written as

$$\kappa^2 = \left(\cos\theta_T - 3\cos\theta_D \cos\theta_A\right)^2 \qquad (1\text{-}3)$$

where θ_D and θ_A are the angles between the line connecting centers of the dyes and the transition moments of the donor and the acceptor, respectively, and θ_T is the angle between the transition moments μ_D and μ_A (Figure 1-3B). (More details on its derivation are provided in Chapter 2).

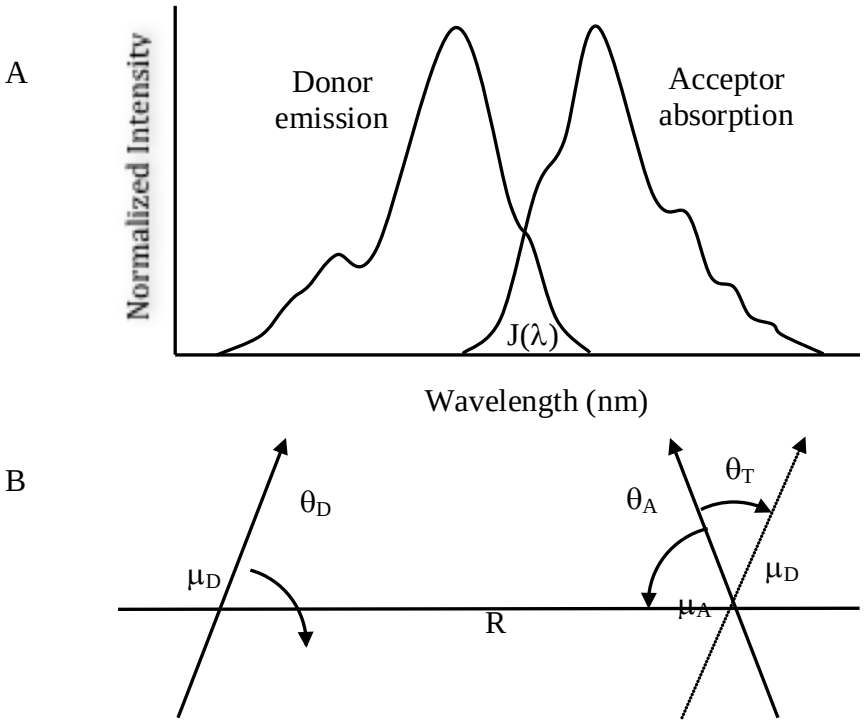

Figure 1-3. Förster radius parameters. A) Spectral overlap, J(λ). B) Orientation factor, κ^2.

The advantage of Förster's equation is that all of the parameters can be determined from the properties of the donor and acceptor individually except for the two structural parameters, κ and R. While this formula has proven to be extremely useful, its derivation involves a number of assumptions that often limit the detail with which structural information can be extracted from FRET data. These approximations include:

1) The coupling between the donor and acceptor is assumed to be in the weak regime, meaning that the excited states of the FRET system are approximately the same as the independent donor and acceptor.

2) The donor is in an excited electronic state that is vibrationally relaxed.

3) The coupling between the donor and acceptor is described by a dipole–dipole interaction.

In most cases, two additional assumptions are employed.

4) Both the donor and acceptor sample all possible relative orientations on a timescale that is rapid compared to the energy transfer timescale, in which case the average value of $\kappa^2 = 2/3$.[35]

5) The rates of other kinetic pathways in the system, k_{OP}, remain constant on the timescale of the experiment allowing E_{ff}, the efficiency of energy transfer,

$$\left\langle E_{ff} \right\rangle = \left\langle \frac{k_{RET}}{k_{RET} + k_{OP}} \right\rangle \tag{1-4}$$

to be averaged statically over time and ensemble and expressed in terms of a simpler distance parameter,

$$\left\langle E_{ff} \right\rangle = \frac{\left\langle k_{RET} \right\rangle}{\left\langle k_{RET} \right\rangle + k_{OP}} = \left[1 + \left(\frac{\left\langle R^6 \right\rangle}{R_0^6} \right) \right]^{-1} \tag{1-5}$$

where R_0, the Förster radius, is the distance at which the efficiency is 50%. Förster radii are tabulated for many D – A pairs[17], allowing Equation 1-5 to be used to model experimental data. It is important to point out that while the quantum yield of the donor in the absence of the acceptor is assumed to be constant, it must be measured for the specific system to which the donor is attached since it can be quite different from the free donor in solution.

1.4 Experimental Measurements

1.4.1 Instrumentation

Fluorescence measurements are performed using a spectrofluorometer. A simplified diagram of such an instrument is presented in Figure 1-4. A commonly used light source is a Xenon lamp, which provides high intensity light over a wide range of wavelengths.[1] Excitation and emission monochromators, through a series of gratings and mirrors reduce stray light and allow selection of the excitation and emission wavelengths. The emission spectrum obtained

represents the wavelength distribution of the emission measured at a single excitation wavelength. The excitation or absorption spectrum reflects the dependence of the emission

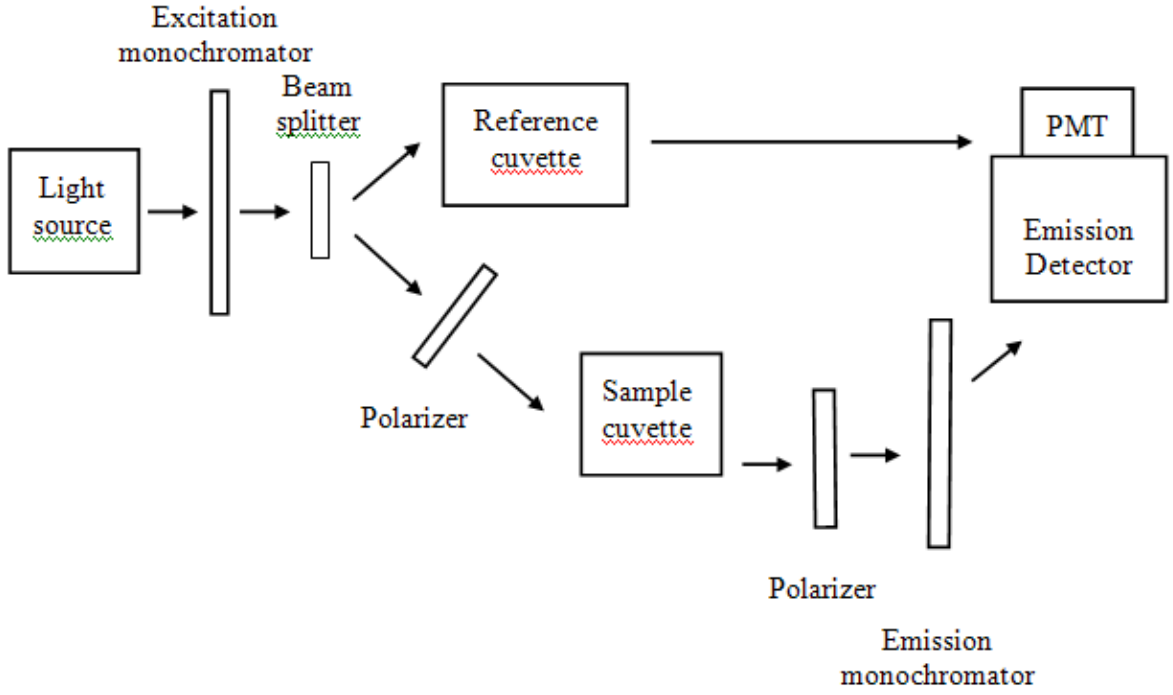

Figure 1-4. Diagram of a basic spectrofluorometer.

intensity on the excitation wavelength at a single emission wavelength.[1] A photomultiplier (PMT) serves as a detector by converting emitted light intensity into current. There are several other features that are commonly included in the instrument. A beam splitter is placed in the excitation path to reflect part of the light into a reference cell containing a stable fluorophore. In this way, any fluctuation in the excitation light intensity can be corrected for by dividing the sample signal by that of the reference. Another component is polarizers, which allow to polarize excitation and select fluorescence intensities with polarization parallel and perpendicular to the excitation polarization.

1.4.2 Quantum Yield

The quantum yield (Q) is defined as the ratio of the number of photons emitted to the number of photons absorbed. It can also be defined as a ratio of the rate constants of radiative deexcitation processes, k_{rad}, to the sum of all of the rate constants,

$$Q = \frac{k_{rad}}{k_{rad} + k_{other}} \tag{1-6}$$

Experimentally, the quantum yield is calculated based on the following formula[1],

$$Q = Q_R \frac{I}{I_R} \frac{OD_R}{OD} \frac{n^2}{n_R^2} \tag{1-7}$$

where I is the area under emission peak (integrated intensity), OD is the optical density and n is the refractive index. The subscript R defines the same properties for a reference fluorophore whose quantum yield is known. The optical density is defined by the Beer-Lambert law,

$$OD = \log \frac{I_0}{I} = \varepsilon c d \tag{1-8}$$

where I_0 is the incident light intensity, I is the transmitted light intensity, ε is the molar absorption coefficient (M^{-1} cm^{-1}), c is the concentration (mol/L) and d (cm) is the thickness of the sample.

1.4.3 Emission Lifetime

The emission lifetime, τ, is defined as the average time a molecule spends in an excited state before returning to the ground state, which depends on rate constants of both radiative and nonradiative processes,

$$\tau = \frac{1}{k_{rad} + k_{other}} \tag{1-9}$$

There are two common ways to measure lifetime: time-domain and frequency-domain.[1] In time-domain measurements, often performed using Time Correlated Single Photon Counting (TCSPC)[36], a sample is illuminated briefly with an excitation light pulse and the time between

this event and an emission of a photon is recorded.[1] After many pulses, a probability distribution of counts versus time is obtained and fitted to a single- or multiexponential curve,

$$I(t) = \sum_i \alpha_i \exp(-t/\tau_i) \tag{1-10}$$

where t is the time after absorption, τ_i are individual decay times, and the α_i, parameters, known as preexponential factors, are the amplitudes associated with each decay time. The sum of the α_i, parameters is normalized to unity. In frequency-domain measurements, intensity-modulated light is used instead of pulsed light. Since molecules spend a finite time in the excited state, there is a phase delay in the emission with respect to excitation. The phase angle and modulation represent the frequency response of the system and are used to calculate lifetimes.

1.4.4 Efficiency of Energy Transfer

While lifetimes and quantum yield are properties of a single fluorophore, either free or attached to another molecule, the efficiency of energy transfer is necessarily a property of a pair of dyes. This efficiency can be calculated in several ways[5], using either lifetime measurements (Equation 1-11) or ratiometric intensities[37] (Equation 1-12),

$$E_{ff} = 1 - \frac{\tau_{DA}}{\tau_D} \tag{1-11}$$

$$E_{ff} = \frac{I_A}{\gamma I_D + I_A} \tag{1-12}$$

where τ_{DA} and τ_D are fluorescence lifetimes of the donor in the presence and absence of the acceptor, respectively, while I_A and I_D are the fluorescence emission intensities of the acceptor and the donor and γ is a correction factor that accounts for the detector response and differential quantum yields of the two channels and is most often set equal to one. The latter approach is illustrated in Figure 1-5, where upon donor excitation, emission intensities of the donor and acceptor, I_D and I_A, respectively, are recorded in separate channels.

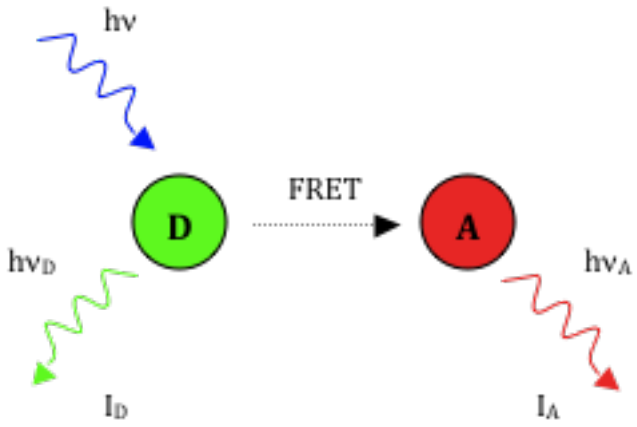

Figure 1-5. Diagram of ratiometric efficiency measurements.

As illustrated in Figure 1-6, the photons emitted by the two probes are counted over a period of time (seconds) and Equation 1-12 is then applied to obtain apparent FRET efficiencies (Figure 1-6B) from which probability distribution histograms and mean values of efficiencies are obtained.

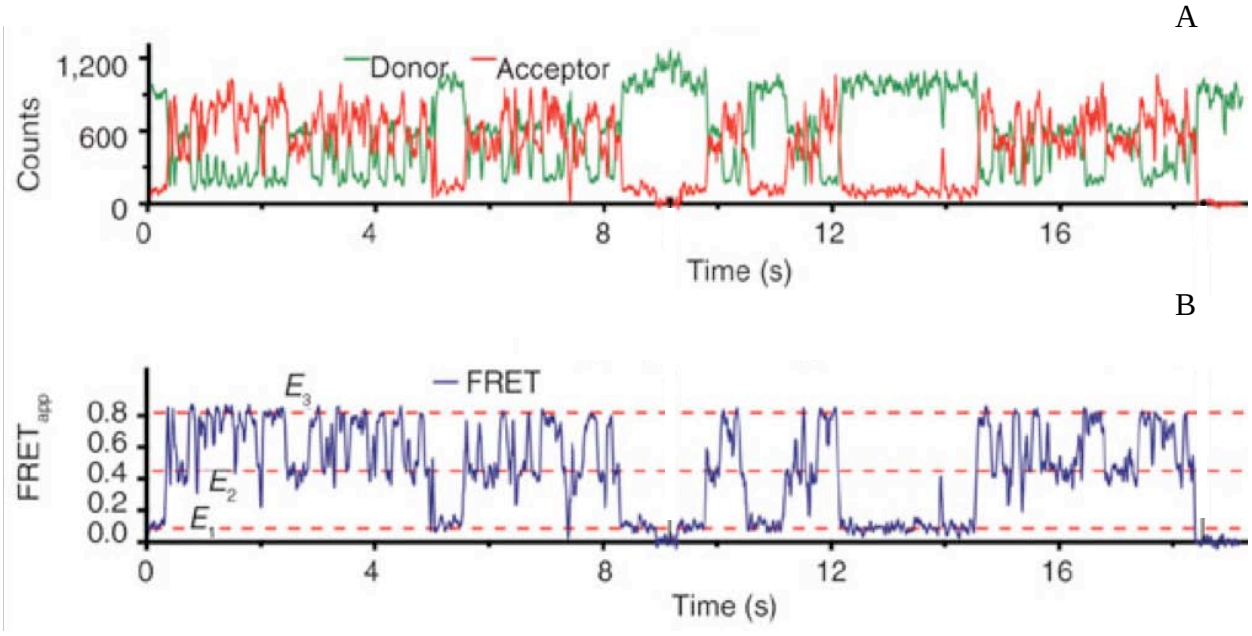

Figure 1-6. Fluorescence Resonance Energy Transfer measurements. A) Fluorescence intensities of the donor and acceptor. B) Apparent FRET efficiency. Reproduced with permission from Roy, R., S. Hohng, and T. Ha. 2008, A practical guide to single-molecule FRET. *Nat. Methods*. 5:507-516, Figure 1b, p. 508.

1.4.5 Anisotropy

Anisotropy measurements provide information about the size and shape of molecules as well as their mobility.[1] The fluorescence anisotropy at time *t* after excitation of fluorophore is calculated using the following equation,

$$r(t) = \frac{I_{\parallel}(t) - I_{\perp}(t)}{I_{\parallel}(t) + 2I_{\perp}(t)} \tag{1-13}$$

where $I_{||}$(t) and $I_{\perp}$(t) are fluorescence intensities of the vertically and horizontally polarized emission, respectively, when the sample is excited with vertically polarized light. The maximum anisotropy value is 0.4[1], which corresponds to the absence of processes that cause depolarization and indicate that the molecule undergoes no rotational movement. One common cause of depolarization is rotational diffusion of fluorophores in the solvent, although, temperature, viscosity, and specific interactions of the probe and the system it labels can affect anisotropy values as well.[38, 39] In fact, most time-resolved anisotropy decays are multiexponential, reflecting a complex interaction of the probe and its environment and are fitted with the following equation,

$$r(t) = \sum_i r_{0i} \exp^{-t/\tau_{ri}} \tag{1-14}$$

where τ_{ri} are rotational correlation times of the fluorophore and r_{0i} are their fractional weights whose sum is equal to 0.4.

1.5 Fluorescent Probes

Most fluorescent probes are rather large (10 to 15 Å across), aromatic, and positively or negatively charged (Figure 1-7). The charge, either as part of the backbone or a side chain, increases the solubility of the probe in water. A lot of conjugation results in larger electron delocalization and lowers the energy of fluorescent transitions to the optical range of light spectrum. Aromatic rings keep the structure rigid and minimize internal rotations that lead to

non-radiative energy decays through internal conversion and vibrational relaxation. Among the most commonly used fluorophores are Cy3 (Figure 1-4B) and Cy5[40], which belong to the

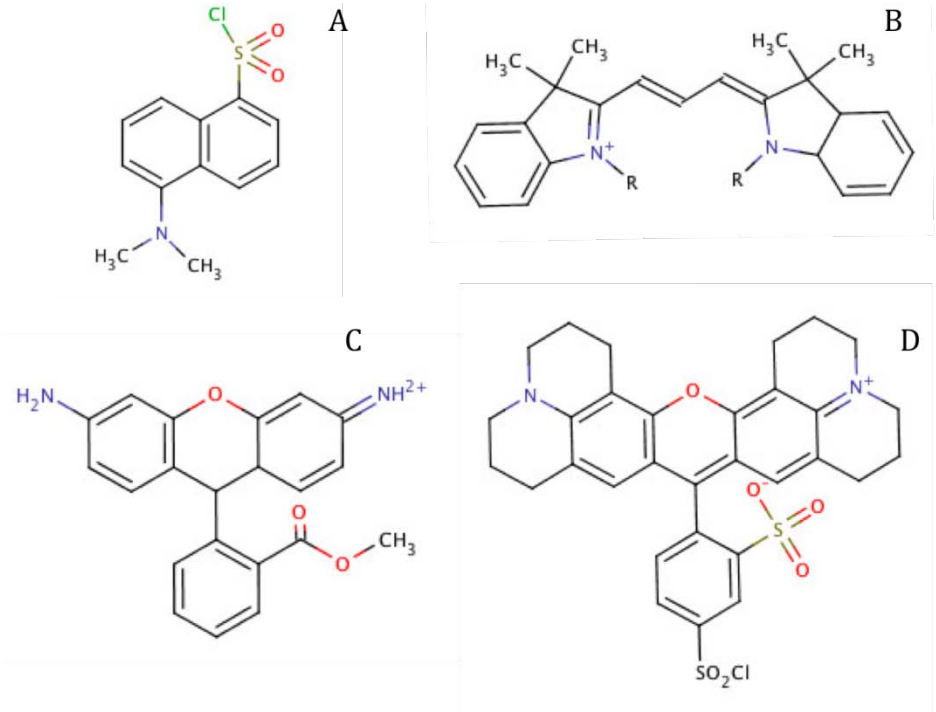

Figure 1-7. Examples of commonly used fluorophores. A) Dansyl chloride, B) Cyanine dye Cy3, C) Rhodamine, D) Texas Red.

cyanine dye family, have high absorption coefficients (> 10^5 M^{-1} cm^{-1}), and are highly photostable. Rhodamine (Figure 1-7C) and Texas Red (Figure 1-7D), as well as the recently introduced Alexa dyes, belong to the rhodamine family. Both families contain dyes that absorb at longer wavelengths than those at which cells autofluoresce, and whose properties are tunable through addition of various side chains. Ideally, fluorophores must be bright (ε > 50,000 M^{-1} cm^{-1}) and have a quantum yield of at least 0.1.[41] Photostability and minimal aggregation effects, as well as good separation between the absorption and emission bands for both donor and acceptor are also desirable properties. Typical fluorophores absorb in the 300 to 500 nm range and emit at 500 to 700 nm.[1] The dyes are connected to the system of interest through amine or thiol reactive groups and long carbon-chain linkers to discourage any specific dye-system interaction.

1.6 Free Diffusion vs. Immobilization

Single-molecule measurements are achieved by either immobilizing the system on a surface or measuring freely diffusing molecules at very low (~100pM) concentrations (Figure 1-8). [5, 37] Both methods have their advantages as well as disadvantages. For example, immobilization of the system allows for studies of dynamics on the millisecond to second timescale. In this case, however, there is always a possibility of surface-system interactions influencing the property of interest. With freely diffusing molecules, on the other hand, it is impossible to study processes that are longer than the diffusion time, on the order of milliseconds. The experimental design, then, is determined mainly by the timescale of the process studied.

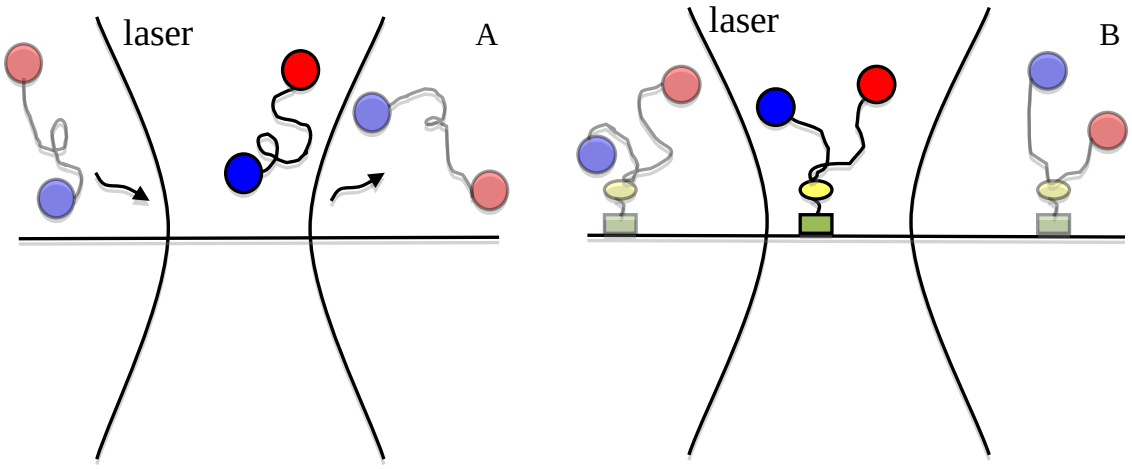

Figure 1-8. SmFRET experimental sample setup. A) Free diffusion. B) Immobilization.

1.7 Important Timescales

Accurate interpretations of experimental results require an understanding of the different processes (and their timescales) that can affect a system's behavior during a measurement of FRET (Table 1-1). As discussed earlier (Figure 1-1), absorption and vibrational relaxation for most systems occur much faster than other processes, and therefore have no effect on fluorescence. The diffusion time becomes important only when the conformational changes are

on a ms scale or longer, which would require immobilization of the molecule. Figure 1-9 illustrates connection between different kinetic processes that affect FRET.

Table 1-1. Important timescales.

Process	Time scale (seconds)	Time scale (prefix)
Absorption[1]	10^{-15}	fs
Internal relaxation[1]	10^{-12}	ps
Lifetime decay[1, 42]	10^{-12} - 10^{-9}	ps – ns
Anisotropy decay[1, 42]	10^{-12} - 10^{-9}	ps – ns
Conformational changes[42]	10^{-12} - 10^{-6}	ps – μs
Diffusion time[43]	10^{-3}	ms
Interphoton time[43, 44]	10^{-6} - 10^{-3}	μs - ms
Bin size[41]	>100μs	μs

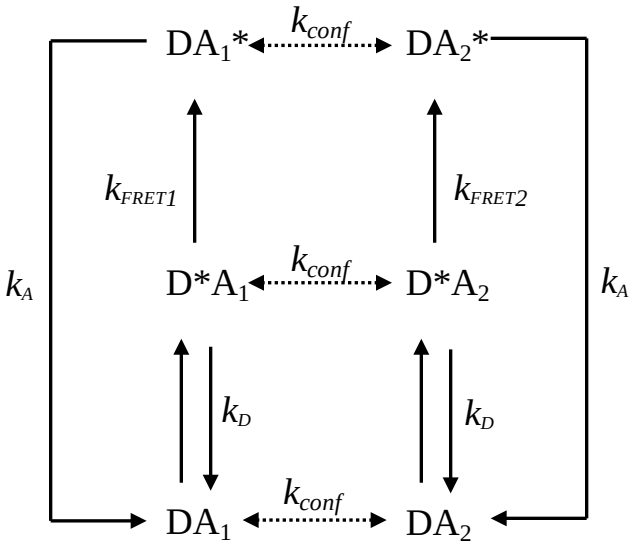

Figure 1-9. Kinetic processes associated with FRET. k_{conf} denotes the rate of conformational change within the system, k_{FRET1} and k_{FRET2} refer to FRET rates of two different system conformations, and k_D and k_A indicate deexcitation rates of the donor and acceptor, respectively.

Aside from conformational fluctuations, there are two parameters related to photon counting that have a direct effect on the calculation of FRET efficiency values. The bin size refers to the time

period for which a single value of efficiency is calculated as a ratio of the acceptor photons in the bin to the total number of photons. The second parameter is the measurement time between two consecutive photons, the interphoton time or τ_{phot}, which is usually in the micro- to millisecond range. For example, suppose a system undergoes transitions between two conformations at the rate of $1/\tau_{conf}$, and the two conformations have distinct lifetimes τ_1 and τ_2. If $\tau_{conf} >> \tau_{phot}$, only one lifetime decay, τ_1 or τ_2, will be observed. If $\tau_{conf} << \tau_{phot}$, both τ_1 and τ_2 will be observed with equal weights. However, if $\tau_{conf} \sim \tau_{phot}$, both τ_1 and τ_2 will be observed but with weights corresponding to the time spent in each conformation.[45]

1.8 SmFRET Nucleic Acid Studies

Structural studies of nucleic acids and their interactions with proteins and each other represent a topic of great interest in the community. Only recently, however, with the emergence of single-molecule methods and smFRET in particular, has it become possible to look in detail at the complicated interactions and conformational changes involved in DNA/RNA binding, melting, folding and many other processes that cannot be extracted easily from ensemble measurements.[10, 29, 46, 47] The use of smFRET in nucleic acid studies was first demonstrated by Ha et al. in 1996.[31] In these experiments, the energy transfer efficiency was measured between tetramethylrhodamine (TMR) and Texas Red fluorophores attached covalently to dsDNA and separated by 10 and 20 base pairs. In 1999, a study by Deniz et al. followed, in which FRET was used to determine molecular distances in dsDNA systems of variable length.[29] This study, which was analogous to Stryer and Haugland's experiment with the polyproline peptide[21], reintroduced the concept of using FRET as a spectroscopic ruler. By demonstrating explicitly the use of FRET in single molecule DNA, this study inspired many additional applications. For example, smFRET has been applied to probe conformational dynamics of a Holliday junction[48], which is a DNA formation that is responsible for genetic recombination during meiosis.

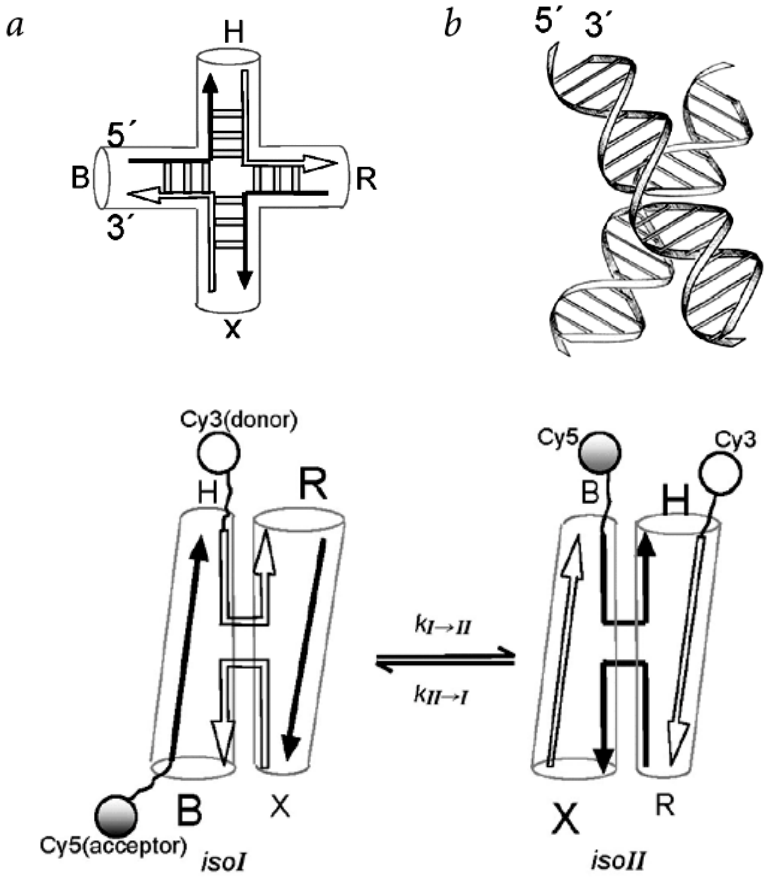

Figure 1-10. SmFRET study of a Holliday junction. Two conformations of the molecule, isoI and isoII corresponding to low and high FRET efficiency, respectively. Reproduced with permission from McKinney, S. A., A.-C. Déclais, D. M. J. Lilley, and T. Ha. 2002. Structural dynamics of individual Holliday junctions. *Nat. Struct. Biol.* 10:93-97, Fig 1, p. 94.

In the experiment, switching between two different conformations of the structure (Figure 1-10) resulted in a change in distance between the donor (Cy3) and the acceptor (Cy5) that, in turn, caused the FRET efficiency to switch from high to low. A different single-molecule FRET study was performed by Tan et al.[49], in which various states of a hairpin ribozyme protein were probed using the Cy3/Cy5 fluorophore pair. Through changes in FRET efficiency during the structural dynamics of the system, it was possible to observe fluctuations of the enzyme between three natural, distinct conformations. Some more recent FRET studies include investigations of a

protein-induced DNA loop conformational switch[50], determination of folding transition times of a single RNA molecule[51], and detection of cofactor binding to dsDNA.[521]

1.9 Objectives of This Work

The examples described above illustrate only a few of the many smFRET applications in which dynamic and structural changes in a system are deduced by monitoring relative changes in the donor-acceptor distance. Absolute distances, however, are almost never considered, despite the quantitative relationship between FRET efficiency and interchromophore distance defined by Förster. Uncertainty in the orientation of the dyes as well as a lack of knowledge about their exact positions with respect to each other and the system preclude accurate distance measurements. Long linkers through which the dyes are attached to DNA, the large size of the probes themselves, as well as the possibility of their interaction with the system, all add to the uncertainty in FRET distances.

This work describes studies of several dye-DNA systems with the goal of elucidating the manner in which fluorescent probes interact with DNA and the effect of these interactions on FRET. Structural fluctuations in interchromophore distances and dipole orientations of the probes, as well as rates and efficiencies of energy transfer are evaluated carefully in the light of the approximations in the Förster model. Theoretical results are compared to available experimental data and possible improvements are proposed in system design with respect to the location and the mode of attachment of the probes.

CHAPTER 2
METHODS

2.1 Molecular Dynamics

2.1.1 Force Field

Molecular mechanics methods describe molecular systems as a collection of nuclei obeying classical, Newtonian laws of motion. This so-called "ball and spring" view of the molecules neglects electronic motion, but enables rapid force and energy calculations. Given an initial set of coordinates, a particular force field equation is applied to calculate the potential energy of the system. Then the force, which is the derivative of the energy with respect to the coordinates, is calculated and the system is propagated to different coordinates. The following equation illustrates the basic force field form used in the AMBER molecular package.[53]

$$U(r^N) = \sum_{bonds} \frac{1}{2} k_b (l - l_0)^2 + \sum_{angles} \frac{1}{2} k_a (\theta - \theta_0)^2 + \sum_{dihedrals} \sum_{n} \frac{1}{2} V_n (1 + \cos[n\omega - \gamma]) + \\ + \sum_{i}^{N-1} \sum_{i<j}^{N} \left\{ \varepsilon_{i,j} \left[\left(\frac{\sigma_{ij}}{r_{ij}} \right)^{12} - 2 \left(\frac{\sigma_{ij}}{r_{ij}} \right)^{6} \right] + \frac{q_i q_j}{4\pi\varepsilon_0 r_{ij}} \right\} \tag{2-1}$$

where U is the potential energy of the system. The first two terms, expressed as harmonic potentials, describe energy changes due to deviations of bonds and angles from their equilibrium values (l_0, θ_0). The third term models the effect of changes in the torsional angles, and the last term which includes Lennard-Jones and Coulombic potentials, represents non-bonded interactions due to van der Waals and electrostatic effects, respectively.[54]

One common algorithm used to propagate velocity and coordinates of a system in a coupled fashion is the leapfrog algorithm,

$$\mathbf{q}(t + \Delta t) = \mathbf{q}(t) + \mathbf{v}\left(t + \frac{1}{2}\Delta t \right) \Delta t \tag{2-2}$$

$$\mathbf{v}\left(t+\frac{1}{2}\Delta t\right)=\mathbf{v}\left(t-\frac{1}{2}\Delta t\right)+\mathbf{a}(t)\Delta t \qquad (2\text{-}3)$$

where ***q*** and ***v*** refer to the coordinate and velocity vectors of all the atoms, whereas acceleration is computed from forces and masses of the atoms.

A typical force field contains a collection of parameters such as force constants, equilibrium bond lengths and angles, and charges that are obtained from experiment or quantum chemical calculations for a particular set of atoms. Selection of these parameters, known as force field parameterization, involves several steps.[54] First, a group of molecules (e.g. proteins, organic) is selected and atom types are assigned based on hybridization and bond-type. Next, parameters such equilibrium bonds and angles, van der Waal radii and atomic charges are measured or calculated using *ab initio* methods. Lastly, a penalty function is defined that assesses the difference between the force field and reference values. Minimization of this function guides the process of selecting a particular set of parameters that correctly reproduces structural or other properties of the system.

2.1.2 Generalized Born Model

All of the simulations described in this work were performed using AMBER 9.0/10.0 software package.[53] The *ff99* force field[55], an all-atom nonpolarizable force field for proteins and nucleic acids, was used for DNA. The parameters for the dyes were computed by the general amber force field (gaff)[56] developed to treat organic molecules. Where possible, we used the generalized Born model (GB)[57] to simulate electrostatic solvent effects. This approach was shown previously to work well for nucleic acids, as compared to explicit solvent simulations, which are much more time-consuming.[58]

The GB model is based on an approximation of the Poisson-Boltzmann equation, which describes solute-solvent electrostatic interaction as the interaction between the solute's charge

distribution and a continuous electric field of the solvent. The GB equation, an adaption of the original Born equation to a many-atom system, describes electrostatic contribution to the free energy of solvation as following[59],

$$\Delta G_{pol} = -\frac{1}{2}\left(1-\frac{1}{\varepsilon_w}\right)\sum_{i,j}\frac{q_i q_j}{f_{GB}} \tag{2-4}$$

where q_i and q_j are partial atomic charges, ε_w is the solvent dielectric constant and f_{GB} is an effective interaction distance,

$$f_{GB}(r_{ij}) = \left[r_{ij}^2 + R_i R_j \exp(-r_{ij}^2/4R_i R_j)\right]^{\frac{1}{2}} \tag{2-5}$$

The interaction distance interpolates between an "effective Born radius" R_i at short r_{ij} distances and r_{ij} at large distances. R_i describes how deeply a charge is buried in the low dielectric medium such as protein or DNA and depends on the intrinsic atomic radii, ρ_i, as well as on the radii and positions of all other atoms,

$$R_i^{-1} = \rho_i^{-1} - \sum_{j\neq i} g(\mathbf{r},\rho) \tag{2-6}$$

In this work we used Bondi radii with additional modifications for different types of hydrogens.[60] Friction effects were simulated with Langevin dynamics described by the following equation,[61]

$$\mathbf{F}_i - \gamma_i \mathbf{v}_i + \mathbf{R}_i(t) = m_i \mathbf{a}_i \tag{2-7}$$

where $\boldsymbol{F}_i$ is the force exerted on atom *i* by all other atoms, γ_i is the friction coefficient (set to 10 ps^{-1}) and $\boldsymbol{R}_i$ is random force that is meant to correct for the absence of explicit collisions with the solvent molecules.

2.2 Transition Density Cube Method

In quantum mechanics, the rate of transition between two eigenstates of a system can be modeled by Fermi's Golden rule, which states that the rate or transition probability, λ_{if}, between

two states depends on the density of final states, ρ_f, and the strength of the coupling between the initial and final states, M_{if}:

$$\lambda_{if} = \frac{2\pi}{\mathrm{h}}\left|M_{if}\right|^2 \rho_f \tag{2-8}$$

This basic equation can be rewritten for a donor-acceptor system by invoking two assumptions of Förster theory: 1) The coupling between the donor and acceptor is in the weak regime, meaning the absorption spectra of the donor and acceptor are unaffected by each other, and 2) the donor is in an excited electronic state that is vibrationally relaxed. The rate constant then becomes:

$$k_{RET} = \frac{2\pi}{\mathrm{h}}\left|V_{DA}\right|^2 J(\varepsilon) \tag{2-9}$$

where V_{DA} is the electronic coupling between the donor and the acceptor in energy units, and J is the spectral overlap of the donor emission and acceptor absorption spectra, normalized on a cm^{-1} scale.[63]

While there are a number of mechanisms that can contribute to the donor-acceptor coupling, the dominant contribution is due to the Coulombic coupling.[25, 64, 89]

$$V_{DA}^{Coul} = \frac{1}{2}\sum_{j,k}\frac{e^2}{\left|\mathbf{R}_{DA} + \mathbf{r}_D(j) - \mathbf{r}_A(k)\right|} \tag{2-10}$$

where $\boldsymbol{R}_{DA}$ is the distance between the centers of mass of the donor and the acceptor and $\boldsymbol{r}_D(i)$ and $\boldsymbol{r}_A(k)$ respectively refer to the coordinates of the jth electron of the donor and the kth electron of the acceptor. Expanding equation 2-10 in powers of $|\mathbf{r}_D(j)\text{-}\mathbf{r}_A(k)|/|\mathbf{R}_{DA}|$ and applying dipole-dipole approximations (only keeping terms up to second order) results in:

$$\langle\psi_D^*\psi_A\left|V_{DA}^{Coul}\right|\psi_D\psi_A^*\rangle \approx \frac{\vec{\mu}_D\vec{\mu}_A}{\left|\vec{R}_{DA}\right|^3} - \frac{3\left(\vec{R}_{DA}\vec{\mu}_D\right)\left(\vec{R}_{DA}\vec{\mu}_A\right)}{\left|\vec{R}_{DA}\right|^5} \cong \kappa^2\frac{|\vec{\mu}_D||\vec{\mu}_A|}{\left|\vec{R}_{DA}\right|^3} \tag{2-11}$$

where $\boldsymbol{\mu}_D$ and $\boldsymbol{\mu}_A$ are transition dipole moments of the donor and acceptor, respectively, and κ_{DA} is the orientation factor expressed as

$$\kappa = \vec{d} \cdot \vec{a} - 3(\vec{r} \cdot \vec{d})(\vec{r} \cdot \vec{a}) \tag{2-12}$$

where $\boldsymbol{d}$ and $\boldsymbol{a}$ are unit vectors pointing in the directions of the transition dipole moments of the donor and the acceptor, and $\boldsymbol{r}$ is a unit vector pointing in the direction of $\boldsymbol{R}_{DA}$.

Applying some additional spectroscopic approximations by relating donor transition dipole moment to donor fluorescence spectrum and the acceptor transition dipole moment to the acceptor absorption coefficient, Förster arrived at his well-known rate equation,

$$k_{RET} = \frac{9000(\ln 10)\kappa^2 Q_D J(\lambda)}{128\pi^5 \tau_D N_A \eta^4} \tag{2-13}$$

in which k_{RET} is the rate constant of resonance energy transfer in inverse time units, κ^2 is an orientation factor between the donor and acceptor transition dipoles, Q_D is the quantum yield of the donor in the absence of the acceptor, τ_D is the lifetime of the donor in the absence of the acceptor in time units, $J(\lambda)$ is the spectral overlap of the emission spectrum of the donor with the absorption spectrum of the acceptor in units of M^{-1} cm^3, η is the index of refraction of the medium, N_A is Avogadro's number in mol^{-1}, and R is the distance between the centers of the donor and the acceptor transition dipoles in cm.

Despite the fact that Förster's dipole-dipole approximation has been generally successful, it is often difficult in experiments to determine whether the donor-acceptor distance is large enough for the model to be valid. The transition density cube (TDC) method[65] offers a solution to this problem by allowing calculation of the full Coulombic coupling, which includes, effectively, higher-order multipole expansion terms,

$$V_{Coul} = V_{dip-dip} + V_{dip-quad} + V_{quad-quad} + V_{dip-oct} + \cdots \tag{2-14}$$

The TDC method solves Equation 2-8 exactly for a given basis. In the TDC method, quantum mechanical calculations are used to determine the ground and excited state wave functions of the donor and the acceptor molecules. These wave functions are integrated to yield the transition densities of the molecule,

$$M_N(r) = \int_S \psi_N \psi_N^* ds dr \tag{2-15}$$

where *N* refers to the donor or the acceptor, in its ground or (*) excited state. The transition densities can then be reoriented to overlay with the D and A position at any given time, *t*, in the MD simulation. The total interaction between the transition density for the donor and that for the acceptor can then be calculated by representing the densities as a 3D grid of charge density cubes and calculating the coupling between each cube $M_D(i)$ of the donor and each cube of the $M_A(j)$ acceptor,rty

$$V_{Coul} = V_{TDC} = \sum_{i,j} \frac{M_D(i) M_A(j)}{4\pi\varepsilon_0 r_{ij}} \tag{2-16}$$

where the sum is over the D and A grids. The coupling calculated in this manner gives the exact Coulombic coupling (in the limit of small cube size, for a given QM model chemistry) for a given configuration, The TDCs are reoriented and V_{Coul} (and $V_{dip-dip}$) calculated for each snapshot from the simulation, yielding a distribution of D – A interactions that represent the effects of structural dynamics in the system.

For all of the systems studied here, calculations of the TDC elements were performed using the Q-Chem[66] software package at the Hartree-Fock level of theory with a 6-31G* basis set. The excited states were determined using Configuration Interaction Singles (CIS) with CIS excited state roots set to 4 and only singlet excited states computed. The number of cube elements was set to 50,000 with test runs with larger values to test convergence.

CHAPTER 3
TMR/CY5 - DNA

Portions of this chapter are adapted from E. Dolghih, A. E. Roitberg, and J. L. Krause, 2007. J. Photochem. Photobiol. A 190:321-327[67] and E. Dolghih, W. Ortiz, S. Kim, B. P. Krueger, J. L. Krause, and A. E. Roitberg, J. Phys. Chem. DOI:10.1021 JP811395, 2009.[68]

3.1 Introduction

3.1.1 Original Experiment

In 1999 Deniz and coworkers[29] used a dsDNA system labeled with tetramethylrhodamine (TMR) and cyanine dye Cy5 to illustrate the use of FRET as a spectroscopic ruler in a single-molecule system. In the experiment, the FRET efficiency between the two chromophores separated by variable number of base pairs was measured and plotted versus modeled Cy5-TMR distances (Figure 3-1).

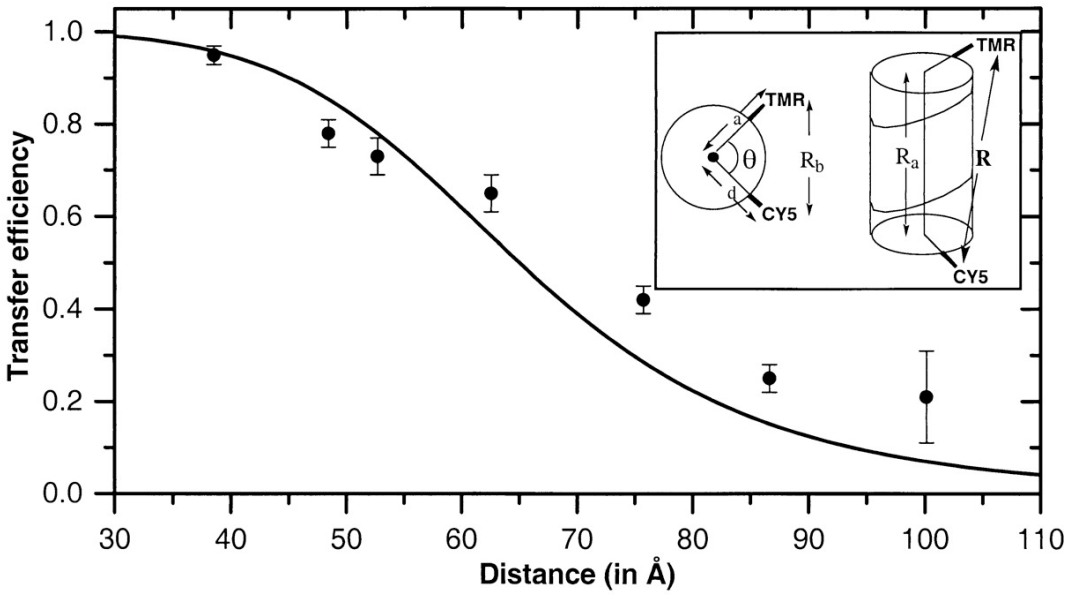

Figure 3-1. Mean FRET efficiencies plotted as a function of distance. Reproduced with permission from Deniz, A. A., M. Dahan, J. R. Grunwell, T. Ha, A. E. Faulhaber, D. S. Chemla, S. Weiss, and P. G. Schultz. 1999. Single-pair fluorescence resonance energy transfer on freely diffusing molecules: Observation of Forster distance dependence and subpopulations. *Proc. Natl. Acad. Sci. USA* 96:3670-3675, Fig. 2b, p. 3672.

The x-axis of this calibration curve was calculated based on the Clegg model of DNA[26] (Figure 3-1, inset) using the following equation,

$$R = ((L + 3.4\Delta N)^2 + (a^2 + d^2 - 2ad\cos(\theta + 36\Delta N))^{1/2} \qquad (3\text{-}1)$$

where L is the separations in distance between the two dyes along the helical axis for zero base pairs, ΔN is the base pair separation, θ is the angular separation between the dyes for zero base pairs, and d and a are the normal distances of the donor and the acceptor to the DNA helical axis, respectively.

In the second part of the study, the authors used smFRET to observe directly distinct subpopulations of DNA structures either in a prepared mixture or produced by enzymatic cleavage or DNA hairpin melting. The ruler was applied to infer the distance separation between the two subpopulations, as depicted in Figure 3-2.

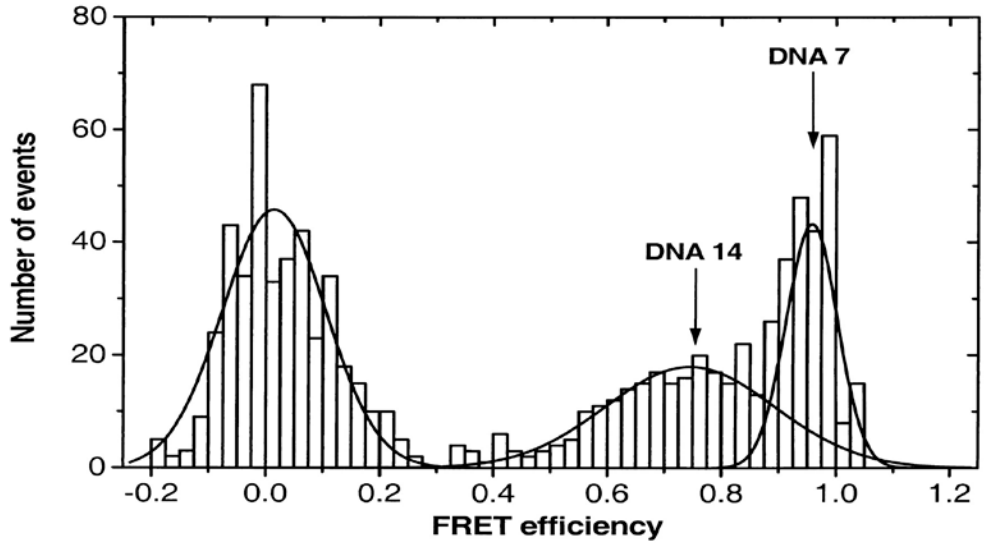

Figure 3-2. FRET efficiency histograms for two DNA complexes of 7 and 14 base pairs. Reproduced with permission from Deniz, A. A., M. Dahan, J. R. Grunwell, T. Ha, A. E. Faulhaber, D. S. Chemla, S. Weiss, and P. G. Schultz. 1999. Single-pair fluorescence resonance energy transfer on freely diffusing molecules: Observation of Forster distance dependence and subpopulations. *Proc. Natl. Acad. Sci. USA* 96:3670-3675, Fig. 3, p. 3673.

The two DNA systems exhibited mean efficiencies separated by 0.2 to 0.3 units, which was found to correspond to ~ 10 Å differences in the distance.

The work by Deniz et al. demonstrates clearly the systematic dependence of efficiency on a single-molecule level on the donor-to-acceptor distance and paved the way for many interesting applications of smFRET to DNA studies. It also, however, revealed potential problems in the use of Förster theory that even decades later, despite the major technological advances and improvements in experimental design, continue to plague the field. For example, in the discussion of the results of the Deniz et al., the authors pointed out a large discrepancy between R_0 = 53 Å as calculated based on spectroscopic data, and R_0 = 65 Å corresponding to the Förster-predicted value. The discrepancy of 12 Å was attributed to the high anisotropy of the probes, as measured in a separate experiment, resulting in $\kappa^2 \neq 2/3$. Another observation that required additional explanation was the broad width of efficiency distributions. The authors proposed that the specific way in which the probe was bound to DNA as the main cause of this effect.

3.1.2 Dye-DNA Interactions

Interactions between fluorescent probes and nucleic acids are known to occur due to electrostatic and hydrophobic forces between charged DNA and aromatic, anionic or cationic dyes.[69-72] Common modes of binding include major and minor groove binding as well as intercalation. While minor groove binders must possess some flexibility to follow the natural twist of DNA, intercalators tend to be cationic and have planar aromatic rings.[69, 71] Some fluorophores, such as cyanine dyes, possess both characteristics and, through small adjustments in their structure or variation in DNA sequence, can bind in either manner.[71] The large variety of dye-DNA interactions, while useful for many other applications, complicates interpretation of smFRET measurements for three main reasons. First, the concept of dyes as free rotors, a crucial assumption of Förster theory, is not applicable. Second, the spectroscopic properties of the dyes, such as quantum yield and fluorescence lifetime, which are assumed in Förster theory to be

constant on the FRET timescale, can be affected by the presence of different modes of binding. If the interchange between the modes happens on a timescale comparable to the rate of FRET, the analysis of the results becomes difficult. Finally, the lack of knowledge of the exact location of the dyes with respect to DNA makes interpretation of mean FRET efficiencies in terms of donor-acceptor distances at best approximate.

Several studies have been conducted with the goal of elucidating the behavior of DNA-bound dyes. One of the earlier of such investigations was performed by Vámosi and co-workers[73] on 5-carboxymethylrhodamine (TMR) covalently linked to the 5'-end of single-stranded (ss) or double-stranded (ds) DNA. Their findings revealed the presence of at least three distinct TMR-DNA states, two of which were fluorescent with lifetimes of 0.5-1 and 2.5-3 ns, and all of which were temperature and ionic-strength dependent, indicating that the photophysical properties of the dye are highly sensitive to the environment. Eggeling et al.[74] proposed a multi-state model for DNA-bound TMR based on three distinct fluorescence lifetimes of 3.6 ns, 2.4 ns, and 0.9-1.7 ns. They described the three states, respectively as TMR exposed mostly to the solvent, TMR interacting with the DNA and TMR quenched by interactions with guanine. The focus of another study, by Dietrich et al.[75] was dsDNA-bound Cy3/Cy5 and TMR/Cy5 donor-acceptor systems. The anisotropy measurement of the dye-DNA complexes indicated that neither Cy3 nor TMR behaved as a free rotor. The biexponential fluorescence decays of the probes suggested the presence of at least two different conformations interchanging on a timescale of milliseconds or longer. Wang et al.[76] also investigated the spectroscopic properties of DNA-linked TMR. Their experiments, performed on a DNA duplex with a single-strand overhang, indicated presence of two TMR states corresponding to a free rotor exposed to the solvent (τ = 3.6 ns), and a state interacting with the DNA on the single-stranded part of the duplex (τ < 1 ns). Fluorescence decay measurements by Unruh et al.[77] confirmed the multiple-

conformation model of DNA-bound TMR (using a carboxylic acid of TMR – TAMRA). Based on fluorescence decay and anisotropy measurements, they proposed a three state-model for the dye; two states rotationally coupled to DNA with short and long fluorescence lifetimes, and a state with the dye as a free rotor and a long lifetime.

For experiments using cyanine dyes in FRET experiments, one of the most highly cited study is that of Norman and coworkers,[78] in which the authors used FRET and NMR analysis to show that carbocyanine dye Cy3, when attached to 5'end of dsDNA through a six-carbon linker, assumes a stacked conformation on top of the molecule. The study, for the first time, provided a clear picture of the nature of the Cy3-DNA interaction that previously was only guessed, based on anisotropy measurements. The experiment showed that it is possible to determine the exact location as well as orientation of a probe with respect to DNA, and hence offered a starting point for more refined FRET measurements of distance. Recent NMR studies by Iqbal and coworkers showed a similar behavior for the carbocyanine dye Cy5.[79] However, their fluorescence lifetime measurements indicated that a fraction of the probes adopted unstacked conformations.[80]

As can be seen from the studies described above, anisotropy and rotational correlation time measurements serve as main tools for providing information about the degree of a probe's rotational freedom. These measurements, more often then not, indicate some interaction between the probes and DNA, but offer no information as to the nature or the extent of this interaction. Theoretical studies have the potential to provide the missing information, but surprisingly few have been performed to date. A docking study, implemented by Unruh et al.[77], revealed that Texas Red had a preference for minor groove binding. Short molecular dynamics of the docked complex indicated that bonding of the dye in this conformation is very stable. Lorenz and coworkers performed a conformational search using the *parm99* force field within AMBER

4.1 package to obtain a distribution of TMR positions at the end of the helix. They found that TMR interacted with major groove and stacked on top of DNA.[81]

3.1.3 Goals of the Study

In reviewing the extant literature, it is apparent that significant uncertainty exists concerning the positions of the dyes with respect to DNA as well their relative orientations. The goal of this work is to investigate this issue by performing molecular dynamics simulations of TMR and Cy5 dyes attached to DNA. In addition to obtaining data that are difficult to determine experimentally, the simulations illustrate how fluctuations in distance and orientation of the dyes affect the interpretation of smFRET results via Förster theory. The critical role of modeling in determining donor-to-acceptor distance is also demonstrated.

3.2 System and Methods

The system studied consisted of the donor-acceptor-labeled double-stranded DNA considered in the experiments of Deniz et al.[29] The donor, tetramethylrhodamine (TMR) was attached with a six-carbon tether to the 5'-end of DNA strand with the following sequence: 5'-CTCTTCAGTTCACAGTCCATCCTATCAGCCGCTTGCCTTC-3'. The acceptor, a carbocyanine dye Cy5, was attached at locations *n* (*n* = 7, 12, 14, 16, 19, 24, 27) of the opposite strands. To decrease simulation time, rather than modeling the full 40 base-pair sequence used in the Deniz et al. experiments, six additional base pairs were included after each Cy5 dye. Control runs with a 33 base-pair DNA sequence showed no difference in the results. The dyes' charges were assigned in the *antechamber* module of AMBER using the AM1-BCC model developed to reproduce restrained electrostatic potential (RESP) charges. DNA molecules were created in the *nucgen* module based on standard B-DNA geometry. Generalized Born implicit solvent model was used to simulate electrostatic solvent effects. We set a cutoff of 20.0 Å for the non-bonded interactions. The ionic strength was set to 0.2 M. The SHAKE algorithm was employed to freeze

the fastest motion in the system – hydrogen stretching – permitting the use of a larger time step of 2 fs. For system equilibration we followed procedures similar to those used typically in DNA simulations.[58, 62] First, structures were restrained harmonically with a 5 kcal/(mol Å^2) force constant and minimized for several cycles, while gradually lowering the restraint to 1 kcal/(mol Å^2). Then, the molecules were equilibrated for 60 ps, while increasing the temperature to 300 K. Finally, the production run was initiated at 300 K, without any restraints. The results were recorded every 1000 steps. The length of the runs was 20 ns, with longer runs performed to test convergence.

For each frame, the orientation factor κ^2 and, consequently, Förster radius were calculated and then averaged over all frames for each run. The following values for the Förster radii calculations for the TMR-Cy5-DNA system were used: $J = 9.9 \times 10^{-13}$ cm^3/M[82], $n = 1.33$[82], and $\Phi_D = 0.56$.[83] For TDC rate calculations, the spectral overlap was determined from experimental spectra $J = 1.26 \times 10^{-4}$ cm.[76, 84] Note that the value of J in the Förster model is different from that in the TDC, as it is normalized differently and has different units. The transition moments of the two dyes were assumed to lie along their long axis.[110]

3.3 Results and Discussion

3.3.1 Conformations and Distance Distribution

Results of our simulations indicate that the dynamics of both TMR and Cy5 are coupled to the dynamics of the DNA molecule. TMR is found to bind in the minor groove of DNA, occasionally assuming a stacked conformation on top of the molecule. Cy5 is observed to bind in two primary locations in the major groove, an upper position, and a lower position (Figure 3-3). These findings confirm previous reports of high anisotropy values for both fluorophores.[29, 74-77] They also support, in part, the docking results of Unruh et al. involving TMR.[77] The tendency of TMR to assume two slightly different positions with respect to DNA agrees with experimental

reports of at least two lifetimes reports for this dye.[73, 74,76] The flexibility of the six-atom linker appears to allow Cy5 to bind in two different locations in the major groove, resulting in an average interdye distance difference of 8 Å between the two conformers. Both probes fluctuate between their different positions within the nanosecond timescale of the simulations, without a

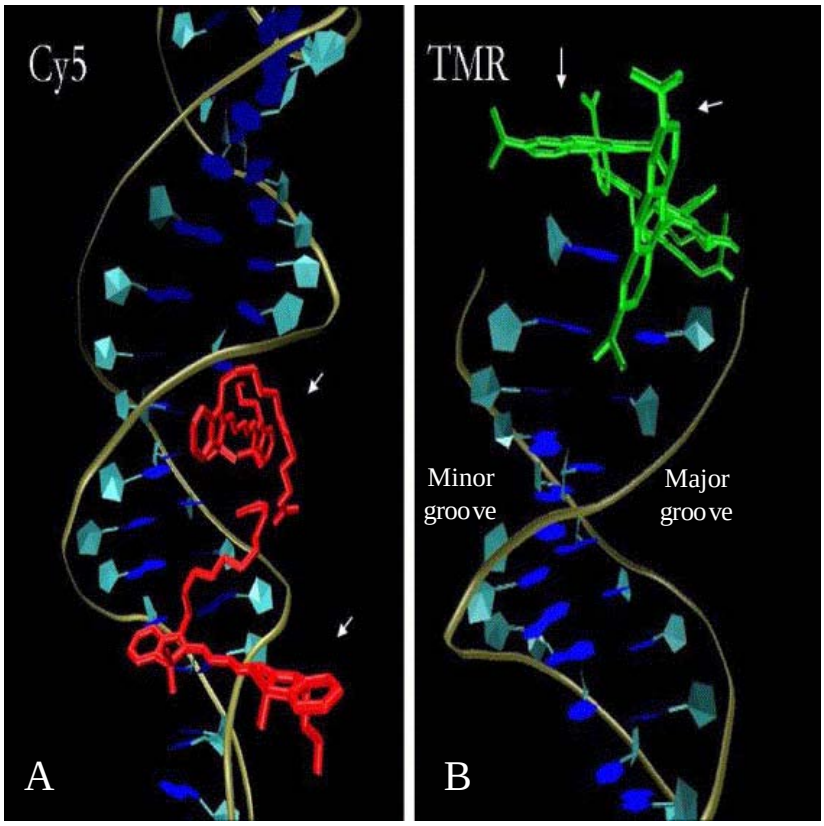

Figure 3-3. Dye conformations in DNA. The acceptor, Cy5 (A) interacts with major groove of DNA in two main conformations, an upper configuration and a lower configuration (marked with arrows). The donor, TMR (B) interacts with the minor groove of DNA or in a stacked configuration (marked with arrows).

noticeable change in the total potential energy of the system. Although the simulations probably greatly underestimate the transition time, these results suggest that the different conformations of Cy5 occur with nearly equal frequency on the timescale of experimental measurements (milliseconds).

As discussed above, to model TMR-Cy5 distance, Deniz and coworkers employed the Clegg model of DNA, which relies on standard B-DNA geometry for all but two parameters (*a* and *d*) that describe the distances between the centers of the fluorophores and DNA long axis (Equation 3-1). These parameters are usually estimated, and supported, at best, by fluorescence anisotropy studies. The parameters vary from 15 Å, corresponding to both dyes fully extended away from DNA to 0 Å, implying close interaction with the DNA molecule. In their distance calculations, Deniz and co-workers assumed the dyes to be free rotors, setting $a = d = 15$ Å. Interestingly, their anisotropy measurements gave a value of $r \sim 0.2$ for both probes, suggesting that rotation of the dyes was hindered significantly. To investigate which set of parameters, if any, would appropriately describe the system being studied, we measured the distances between the centers of the probes throughout the molecular dynamics simulations. The values were averaged for each dye-DNA complex with an assumption that both Cy5 conformations occur with equal frequency (Table 3-1).

Table 3-1. Interchromophore distances as calculated with the Clegg model vs. distances obtained from the simulations (± standard deviation).

N_{bp}	**Clegg Model ($d = a = 15$ Å)**	**Clegg Model ($d = a = 0$ Å)**	**MD (Å)**
7	38.5	28.8	20.7 ± 1.4
12	48.4	45.8	46.1 ± 3.5
14	52.6	52.6	48.9 ± 8.8
16	62.5	59.4	49.6 ± 5.3
19	75.7	69.6	68.8 ± 4.8
24	86.6	86.6	82.1 ± 4.1
27	100.1	96.8	88.9 ± 6.7

For comparison we provide distances predicted by the Clegg model for fully extended dyes as well as for dyes interacting closely with DNA. Average MD distances reported in the table

represent an average over all frames for each system of the distance between the centers of the donor and the acceptor. These values are correct within the Förster's dipole-dipole approximation of the two dyes and assuming their transition dipole moments lie along their long axis.[110] As can be seen in the table, the distances obtained from the simulations, while in general smaller than those predicted by either of the theoretical models, fit more closely to the second model, with an average uncertainty of 5 Å. This is not surprising, since the dyes are observed to interact with the DNA throughout the dynamics. However, even with the $a = d = 0$ Å assumption, the average distances for some of the systems differ by 8 to 10 Å from those observed in simulations, which is not surprising since the size of the dyes is ~10 Å. The presence of multiple conformations of Cy5 can certainly contribute as well to this result.

3.3.2 Efficiencies

Using distances and κ^2 computed for each frame of molecular dynamics, we applied Förster formula to calculate average efficiencies for each oligonucleotide. As shown in Figure 3-4, the calculated efficiencies are in an excellent agreement with the mean experimental efficiencies reported by Deniz et al., when plotted versus the values of *R* determined from the simulations. In the figure, the original experimental data is indicated by open circles, average MD efficiencies are shown as red squares, and experimental efficiencies plotted vs. MD distances are shown as black circles. Theoretical and experimental data are fitted with the Förster formula to obtain R_0. Note, that the theoretical values at large distances are in worse agreement with the experiment than those at short distances. There is, however, significant uncertainty in experimental mean efficiency values at longer donor-acceptor separations, where efficiency values are close to zero and therefore are difficult to separate from the peak at zero due to acceptor photobleaching. When fitted to the Förster formula, the theoretical data indicate an R_0

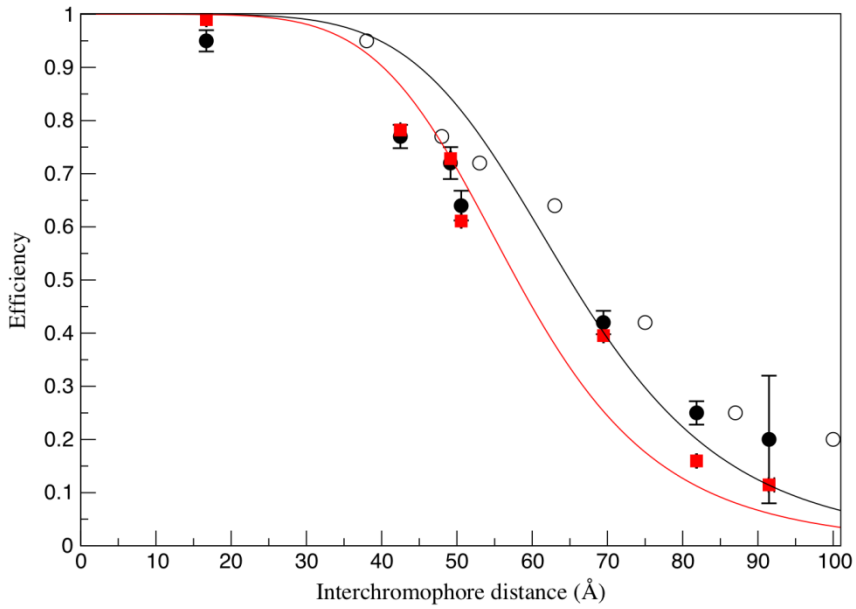

Figure 3-4. Förster efficiencies. Experimental efficiencies vs. modeled (empty circle) and average MD (black circle) distances. Theoretical efficiencies vs. average MD distances (red squares) calculated as explained in the text. Förster fit of experimental data (black curve), R_0 = 65 Å, and theoretical data (red curve), R_0 = 58 Å. Standard errors of theoretical averages are included.

value of 58 Å. This value is in a better agreement with R_0 = 53 Å (estimated from spectroscopic data) then R_0 of 65 Å fitted by Deniz et al. Surprisingly, if we re-plot both sets of data using Equation 3-2, it becomes apparent that neither set of data are represented well by an R^{-6} dependence (Figure 3-5).

$$\ln\left(\frac{1}{E_{ff}}-1\right)=m\ln\left(\frac{R}{R_0}\right) \qquad (3\text{-}2)$$

Shown in the figure are four lines. One plots the experimental data (solid triangles), using the values of *R* obtained from the Clegg model. This line has a slope of 4.3. A second line plots the results of the simulations, with the Cy5 fixed in one of its conformations, and the values of *R* determined from MD (solid circles), with an average R_0 determined from the simulation. This

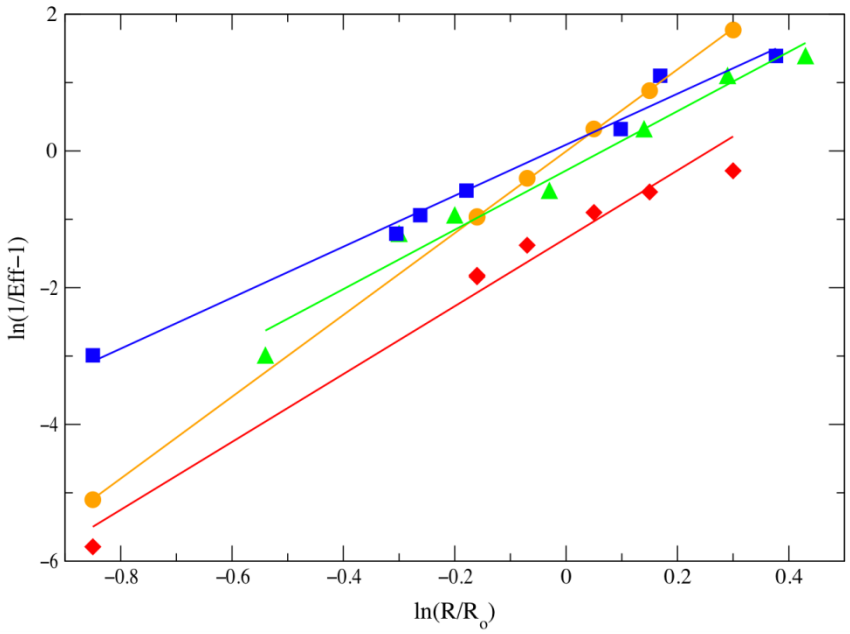

Figure. 3-5. Effect of multiple fluorophore conformations on Förster-predicted R^{-6} dependence, as explained in the text.

line has a slope of 6.0, as it must, since the efficiencies are determined using the Förster formula. All average values represent averages over all frames for a given system. A third line (solid squares) shows the experimental efficiencies versus the theoretical values of *R*, with a slope of 3.7. The fourth line (solid diamonds) shows average theoretical efficiencies assuming that the Cy5 adopts two conformations (and that each conformation obeys Förster scaling), as calculated with the following formula:

$$\left\langle E_{ff} \right\rangle = \frac{1}{2}\left(\frac{1}{1+\left(R/R_0\right)^6} + \frac{1}{1+\left(\left(R+\alpha\right)/\left(R+\beta\right)\right)^6} \right) \qquad (3\text{-}3)$$

In this formula, $\alpha = 7.79$ Å is the average difference in distance between the two conformations of Cy5 and TMR, and $\beta = 13.53$ Å is the average difference in Förster radius for the two conformations. The slope of this line is 5.0. While we are not suggesting that this is the correct method to calculate the efficiencies (one would need to do an ensemble average over all

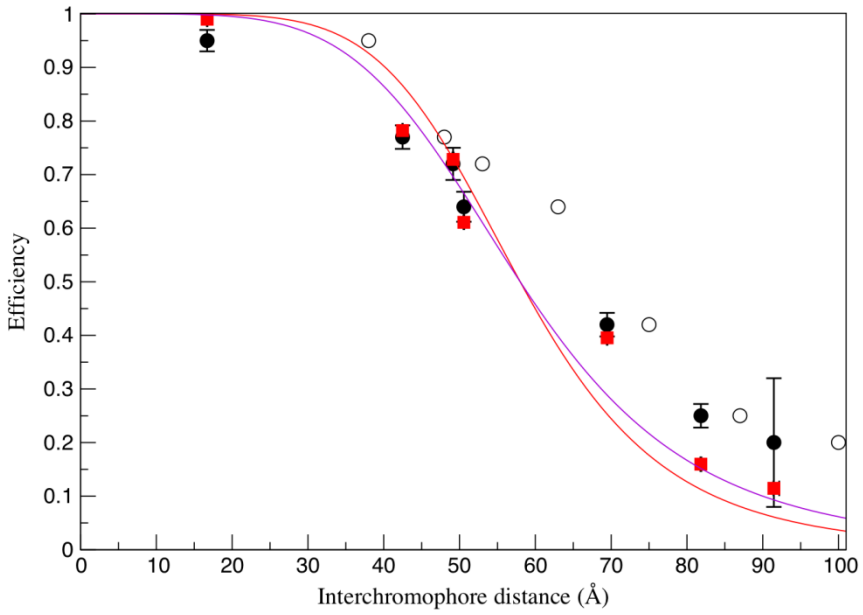

Figure 3-6. Fit of theoretical data with R^{-5} curve (purple) and R^{-6} (red).

conformations adopted by both dyes), Figure 3-6 illustrates that adding a single additional configuration results in a weaker *R* dependence than the Förster-predicted R^{-6}.

3.3.3 Orientation Factor, κ^2

In conventional applications of the Förster formula, the orientation factor, κ^2, is often set equal to 2/3, based on the assumption that the dyes are rotating freely and all dipole orientations are sampled equally. Experimentally, however, there is no guarantee that this is the case. In fact, more often than not, the dyes are involved in some type of interaction with DNA. As our simulations show, both TMR and Cy5 are coupled to DNA in their motion, which results in limited rotational freedom. This hindered motion of the dyes does not have a dramatic effect on the average κ^2 values (calculated for each frame and then averaged for each run) representing averages over time for each system. We find that in most cases $<\kappa^2>$ lies within 45% of 0.67. While this might be an acceptable range of variation, as Figure 3-7 illustrates, similar average values of the orientation factor can correspond to very different distributions. In this figure, the

two distributions (1000 frames each) are obtained from MD simulations corresponding to n =12, and n = 16 DNA systems. The average κ^2 in one case is 0.84, and the other is 0.86. Also shown in the figure is the theoretical distribution derived from the $P(\kappa^2)$ that gives $\langle\kappa^2\rangle = 2/3$.[17]

There are, in general, two ways to look at κ^2 averaging in single-molecule measurements: static and dynamic.[85] Dynamic averaging is applicable when the donor and acceptor sample all allowed orientations before energy transfer occurs.

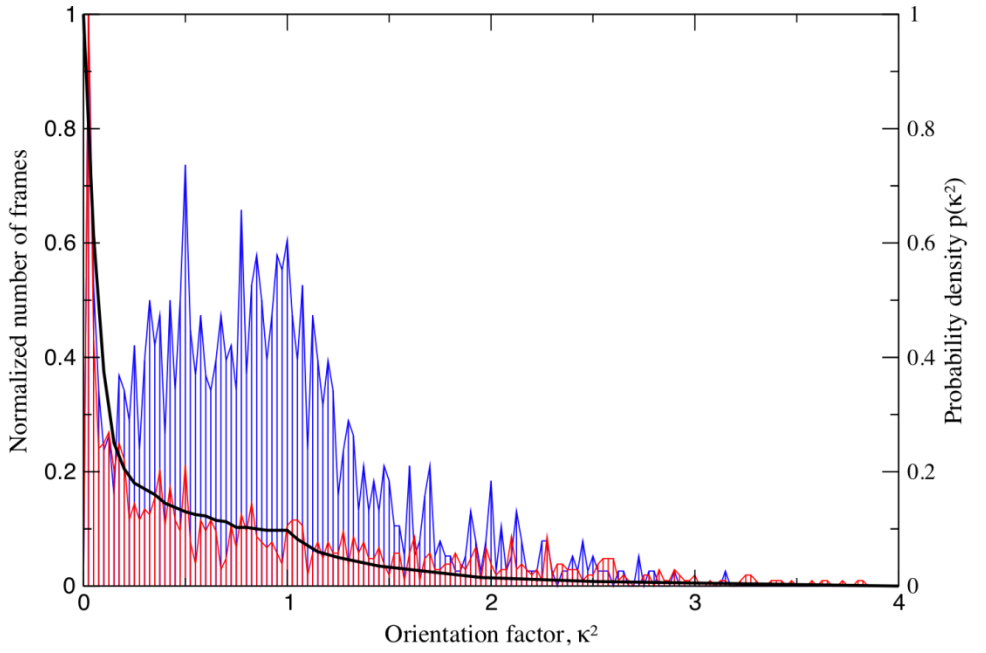

Figure 3-7. Dipole orientation factor, κ^2. Distributions are shown for n =12 and n = 16 simulations, one with an average κ^2 of 0.84 (blue) and the other with an average κ^2 of 0.86 (red). The solid line represents the theoretical prediction for the $P(\kappa^2)$ expected for $\langle\kappa^2\rangle = 2/3$.

In that case efficiency is calculated based on an average κ^2 value.

$$E_{ff} = \frac{\left\langle R_0^6 \right\rangle}{\left\langle R_0^6 \right\rangle + \left\langle R^6 \right\rangle} \tag{3-4}$$

In the static limit, the reorientation of the dyes is slow due to steric or other reasons and the efficiency measurement is dependent on a specific, rather than an average, κ^2 value. In the case

shown in Figure 3-7, the distribution corresponding to $<\kappa^2>$ = 0.86 matches the theoretical distribution for $<\kappa^2>$ = 2 /3 rather closely, while the distribution for $<\kappa^2>$ = 0.84 is completely different. Moreover, as shown in Table 3-2, the two distributions result in different average efficiency values when calculated using the Förster formula. Here, although the mean value of R is slightly different for the two systems, we used a single value in both calculations (an average of one of the runs) so that any observed fluctuation in the efficiency is reflected only in variations in the orientation factor. The first two rows of the table reflect average efficiencies corresponding to the two different distributions of κ^2 (Figure 3-7). The two values were calculated via the following formula,

$$E_{ff} = \left\langle \frac{R_0^6}{R_0^6 + R^6} \right\rangle \tag{3-5}$$

where R = 54.4 Å and R_0 was calculated independently for each frame. Both efficiency values correspond to the static limit.

Table 3-2. Effect of calculated κ^2 on efficiencies.

κ^2	Efficiency (±st. dev.)
0.86	0.65 ± 0.29
0.84	0.56 ± 0.29
0.86	0.84

In the third row, the dynamic limit was applied, and efficiency was calculated as in Equation 3-5 using an average value of R_0^6 based on $<\kappa^2>$ = 0.86 and the same average value of R as above. The table illustrates that using average κ^2 can result in very different, and, in this case, grossly incorrect, efficiencies, compared to those obtained using the true κ^2 distribution.

3.3.4 Rates

In addition to calculating interchromophore distances and orientation factors, we applied the TDC method to calculate rates of energy transfer. In Table 3-3, we compare TDC rates to those calculated with the dipole-dipole approximation of Förster theory. As expected, when the interdye distance is comparable to the size of the dyes ($n \sim 7$), the Förster model overestimates the rate. This should be of significant concern in future work for systems in which the distance between the dyes is relatively short. An additional potential advantage to employing TDC is the ability to predict efficiencies using TDC rate constants and the following equation:

$$E_{ff} = \frac{k_{TDC}}{k_{TDC} + \tau^{-1}} \tag{3-6}$$

where τ is the donor lifetime. This method eliminates the Förster imposed R^{-6} dependence completely. In the case of TMR, however, this might not be of much value, since the dye is known to have several lifetimes when bound to DNA. The uncertainty in experimental measurements due to these different lifetimes would likely result in poor theoretical predictions for this probe.

Table 3-3. FRET rate constants calculated using Förster theory and the TDC method, for varying number of base pairs between the chromophores.

N_{ap}	k_{TDC} (ns^{-1})	$k_{Förster}$ (ns^{-1})
7	54.0	143
12	1.54	4.18
14	2.11	5.34
16	0.72	2.08
19	0.12	0.36
24	0.07	0.20
27	0.03	0.08

3.4 Conclusion

In many FRET experiments performed for systems with dye-labeled DNA, the positions of the dyes with respect to DNA and their relative orientation are unknown, which precludes an accurate application of Förster theory. Our study of a Cy5-TMR-labeled DNA system shows that both dyes interact with DNA and assume multiple conformations that interconvert on the time-scale of the experiment. As a general trend, the average donor-acceptor distances are smaller than the values predicted using standard B-DNA model. This discrepancy, which for some systems is as high as 10 Å, is caused primarily by the presence of two different positions assumed by Cy5 with respect to DNA. Cy5 interconversion between two conformations also causes large fluctuations in both the interchromophore distance and the orientation factor, which results in a broad distribution of experimental efficiencies. In general, the Clegg model is inappropriate for predicting donor-acceptor distances in cases in which multiple conformations of the probes are present. An analysis of the orientation factor averages and distributions indicates that the static, rather than the dynamic, limit of efficiency averaging is the correct approach for this particular system. This conclusion is supported by the evidence of hindered motions of the dyes throughout the dynamics due to interactions with the DNA. Finally, presence of multiple probe conformations results in a weaker R dependence than the Förster-predicted R^{-6}.

CHAPTER 4
STILBENE/PERYLENE - DNA

4.1 Introduction

4.1.1 Orientation Factor

In his original derivation of the theory, Förster incorporated all of the orientation dependence in the FRET process into a single parameter – κ^2.[15,16] The orientation factor is defined on the basis of the orientation of the transition dipoles of the probes and can be written as,

$$\kappa^2 = \left(\cos\theta_T - 3\cos\theta_D \cos\theta_A\right)^2 \tag{4-1}$$

where θ_D and θ_A are the angles between the line connecting centers of the dyes and the transition moments of the donor and the acceptor, respectively, and θ_T is the dihedral angle between the transition moments μ_D and μ_A. The highest value of the parameter is 4, corresponding to the donor and acceptor vectors aligned with the line between their centers.[17] Its lowest value, 0, can be achieved through various orientations, including the case in which the donor and acceptor transition moments are perpendicular to each other and to the center-to-center line. Förster went on to suggest that the orientation parameter, while impossible to measure experimentally, can be assumed to be 2/3, corresponding to freely rotating donors and acceptors that sample all possible orientations (the isotropic limit). The effect of this assumption on the interpretation of fluorescence resonance energy transfer measurements has been a major point of discussion for quite some time. In 1975, Dale and Eisinger[85] provided an interpretation of experimentally measured efficiencies in terms of static and dynamic orientational averaging. In the dynamic limit, the dyes sample all possible orientations before energy transfer occurs, resulting in the same transfer efficiency for each molecule *i* in an ensemble. In such a case, the average efficiency of the ensemble becomes:

$$\left\langle E_{ff} \right\rangle_{dyn} = \left\langle E_{ff}(i) \right\rangle = \frac{\left\langle \kappa_i^2 \right\rangle}{C^{-1}R^6 + \left\langle \kappa_i^2 \right\rangle} \tag{4-2}$$

where R is the interdye distance and C is a combination of spectroscopic and solvent parameters. When the orientation sampling is fast, and not all of the orientations are sampled, lower and upper limits on the average κ^2 can be estimated.

In the case of the static limit, the donor and the acceptor do not change orientation during the transfer due, for example, to steric inhibition or specific interactions within the system studied. As a result, the efficiencies for each molecule are different and the average efficiency of the ensemble becomes,

$$\left\langle E_{ff} \right\rangle_{stat} = \left\langle \frac{\kappa_i^2}{C^{-1}R^6 + \kappa_i^2} \right\rangle \tag{4-3}$$

Based on this model, the authors concluded that in the case of static averaging, ensemble efficiency measurements could not be used to provide meaningful values of the distance. In a later publication, the same authors described an experimental approach for determining the orientation regime of a system and setting limits on $<\kappa^2>$ in the case of dynamic limit through use of fluorescence polarization anisotropy measurements.[86] After the first single-molecule FRET experiment was performed by Saito and coworkers in 1995[87], dos Remedios and Moens[88], addressed the issue again, this time for a single–molecule system. The authors concluded that thermal motions of the protein molecule together with the freedom of motion provided by the tethers of the probes should guarantee a dynamic averaging of the dyes' orientations. There have been several theoretical studies performed as well on the subject. For example, Wong et al.[89], Ortiz et al.[90], and Khan et al.[91] demonstrated the effect of the probe orientation on the rate of energy transfer at short distances as well as at separations larger than R_0.[91] Another study was

performed by VanBeek et al.[92] on a protein with a freely rotating donor and an acceptor in a fixed orientation. Their analysis showed a significant correlation between κ^2 and R, that is

$$\left\langle \kappa^2 R^{-6} \right\rangle \neq \left\langle \kappa^2 \right\rangle \left\langle R^{-6} \right\rangle \tag{4-4}$$

indicating that the dynamic model for efficiency calculations is incorrect in this and similar systems. This confirmed the earlier conclusion of Dale and Eisinger.[85]

4.1.2 Original Experiment

The first experimental study to illustrate the systematic dependence of FRET efficiency on the orientation factor was performed by Lewis et al. in 2005.[93] The system consisted of dsDNA with stilbene dicarboxamide (SA), the donor, covalently attached to both strands forming a hairpin and perylenedicarboxamide (PA), the acceptor, attached to one strand as a 'cap'. Both dyes were assumed to be in stacked positions at the opposite ends of the DNA based on X-ray crystal structure of a similar system[94] (Figure 4-1).

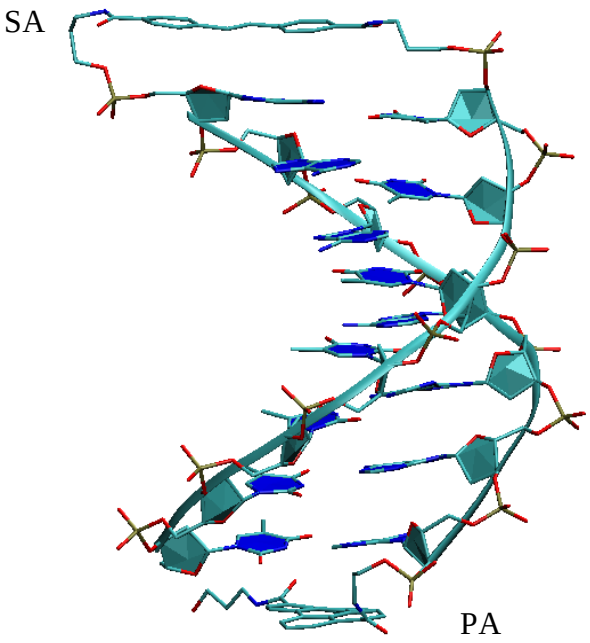

Figure 4-1. Stilbene hairpin structure for N = 7.

In this study, the authors measured lifetimes and quantum yields of the donor at various base pair separations between the two probes and demonstrated the correlation of those properties with the

orientation factor (Figure 4-2). The interchromophore distance was modeled with ((*N*+2)*3.4) Å, where *N* corresponded to the number of intervening base pairs and 3.4 Å standard base pair separation was assumed. The dyes were estimated to add to the separation in a manner of two additional base pairs. Modeling of κ^2 factor is less clear. While the text description of κ^2 calculation implies that the orientation factor was computed assuming SA-DNA twist angle of 17° from X-ray crystal structure and 0° angle for PA, calculated κ^2 value in Figure 4-2 is inconsistent with that description. In a separate study, the authors used DNA with two stilbene

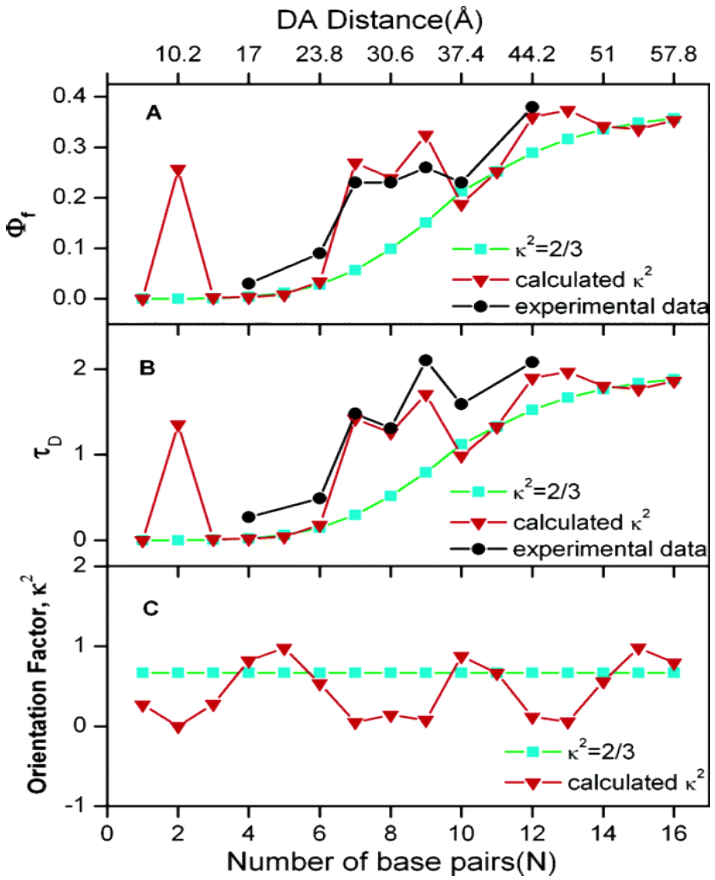

Figure 4-2. Quantum yield, Φ_f, lifetime, τ_D, and orientation factor, κ^2 vs. number of base pairs, N. Reproduced with permission from Lewis, F. D., L. Zhang, and X. Zuo. 2005. Orientational control of fluorescence resonance energy transfer using DNA as a helical scaffold. *J. Am. Chem. Soc.* 127:10002-10003.

probes attached at the opposite ends to illustrate the use of circular dichroism for obtaining donor-acceptor distances.[10] They also employed molecular dynamics to investigate the effects of

fluctuation in distance and orientation of the probes on the CD spectra. The transition moments of the two dyes were assumed to lie along their long axis.[102, 103]

4.1.3 Fluorophores

Stilbenedicarboxamide, attached covalently in a form of cap to DNA, was shown by Letsinger and coworkers[95] to stabilize short helical DNA domains in the form of a hairpin (Figure 4-3). The original interest in creating such structures was related to their potential use in enzyme binding and catalysis, as well as in development of various DNA assemblies. The dye is

A

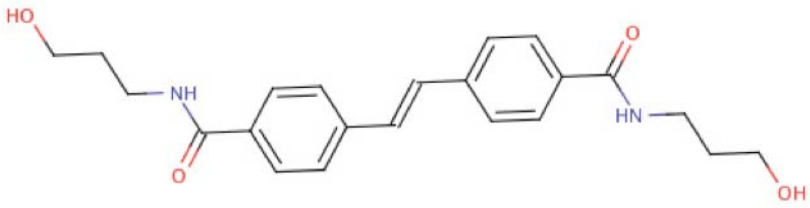

B

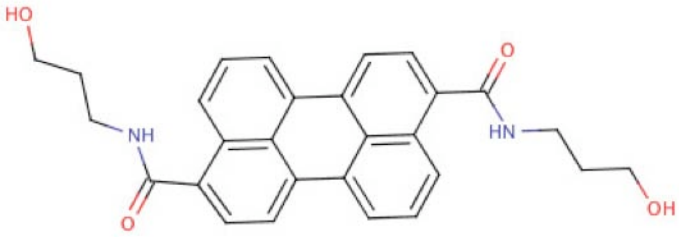

Figure 4-3. Capped hairpin fluorophores. A) Stilbene dicarboxamide, SA.
B) Perylenedicarboxamide, PA.

known to have absorption and emission maxima at ~330 and ~390 nm, respectively. Perylenedicarboxamide absorbs strongly in the visible part of the spectrum with a maximum at 450 nm. Its emission maximum is at 500 nm. SA's quantum yield is increased by conjugation to DNA from 0.17 to 0.38.[96] It should be noted that there have been several studies involving electron transfer in stilbene hairpins.[97,98,99] In these systems, however, SA served as an electron acceptor, and an electron donor, such as stilbene diether or a G-C pair, was included as well.

4.1.4 Goals of the Study

For more sophisticated FRET distance measurements, Lewis et al. suggested a system that could provide rigid control over the orientation and position of the dyes. Using molecular dynamics and the Transition Density Cube method, we studied various structural aspects of this system, the dynamic fluctuations, and the effects of these fluctuations on the interpretation of experimental data, such as fluorescence lifetimes, quantum yields and efficiencies.

4.2 System and Methods

The systems simulated consisted of polyA-polyT DNA duplexes of length *N* (*N* = 1 to 15) with a donor, SA and an acceptor, PA covalently attached by tethers at the opposite ends of DNA in a stacked position. Initial attempts at simulating the system in implicit solvent failed due to fraying of the end base pairs, an event not uncommon in implicit solvent simulations. To overcome this difficulty, the production runs were repeated in an explicit solvent. Partial atomic charges of the two probes were obtained using the RESP (restrained electrostatic potential) charge-fitting method[100] after optimizing the geometries with Hartree-Fock and a 6-31G* basis set in Gaussian.[101] The systems were minimized initially in implicit solvent (GB model) and then equilibrated for 60 ps while DNA was restrained with 25 kcal/mol$Å^2$ force constant. Next, the system was solvated in octahedral solvent box of ~ 1000 to 4000 water molecules and the solvent was equilibrated for 40 ps while increasing the temperature from 0 to 300 K. The DNA complex was restrained with 10 kcal/mol$Å^2$ force constant. The entire system was then equilibrated with no restraints, at a constant pressure, for 100 ps. The production run was implemented with a 2 fs time step and simulated for 4.5 ns, of which the last 3.5 ns were analyzed. Results were saved every 1 ps and every 2nd frame was further analyzed. Distances, orientation factors, and transfer rates were calculated with the TDC method for each frame and then averaged.

4.3 Results and Discussion

An evaluation of the molecular dynamics showed little fluctuation (< 5%) in the interchromophore distance throughout the simulation time (Figure 3-4). The distance was found to depend linearly on the number of base pairs and was fitted with the equation R = 4.83(±0.04) + 3.24(±0.9)*(N-1), where *N* is the number of base pairs, 3.24 Å is the rise per base pair and 4.83 Å is the additional rise due to the two dyes. Figure 4-4B shows the distance distribution for the *n* = 11 system, over the first and second halves of the simulation. They overlap almost perfectly,

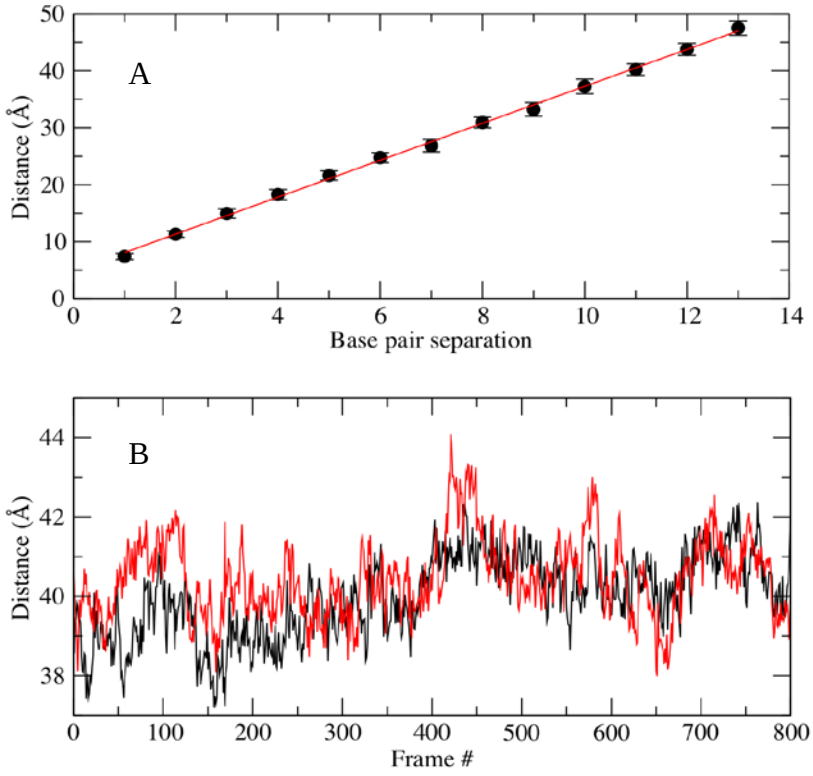

Figure 4-4. MD distance analysis. A) Average SA-PA distance from MD with standard deviation. B) Distance distribution for n = 11 over first (black) and second (red) halves of the run.

indicating that the simulation is converged with respect to the interdye distance. Little fluctuation was noticed in the angles between the dyes and the long axis of DNA. Experimental measurements have shown that SA and PA transition moments lie along their long axis.[102, 103] Thus, θ_A and θ_D for SA and PA were 95.0±6.4° and 93.1±3.5°, respectively, (Figure 4-5B) indicating that the dyes remained in a stacked position, almost perpendicular to the long axis of

DNA throughout the run. The dihedral angle between the two dyes increased in a manner reflecting the helical structure of the DNA (Figure 4-5A). The linear fitting result was found to be: θ_T= 68.4(±4.3°)+30.0(±0.54°)N, where *N* is the number of intervening bases, 30.0° is rotation per base pair and 68.4° is a combined twist angle of the two probes. The systems' parameters compared well with the standard B-DNA parameters

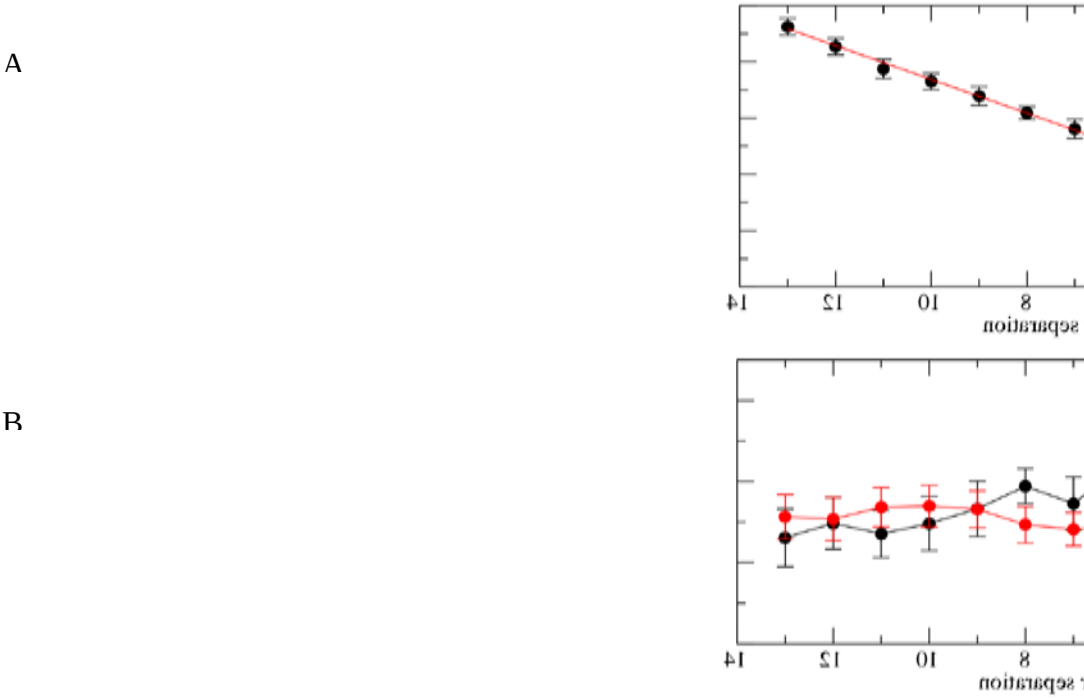

Figure 4-5. Orientation factor angles for SA and PA. A) Average θ_T for each run with standard deviation. B) Average θ_D (red) and θ_A (black) angles with standard deviation.

of 3.32±0.19 Å for rise per base pair and 35.9±4.2° for rotation per base pair as suggested by Dickerson et al.[12] The average angle between SA and its adjacent base pair was 24.3±8.3°, which is slightly larger than the value of 17° obtained from the X-Ray crystal structure, and used by Lewis et al. to calculate κ^2.[88] (Figure 4-6) This value, however, is smaller then the average value of 34° obtained by Lewis and coworkers from MD simulations in another study.[95] The corresponding angle for PA was 68.0±11.4°, which differs from the value of 0° used by Lewis et al. to fit theoretical data to the experiment. Note, that both dyes exhibit an approximate standard

deviation of 10° in the twist angle, and that PA is more flexible than SA due to its single point of attachment. The deviation increases for SA at longer separations, indicating an increased overall

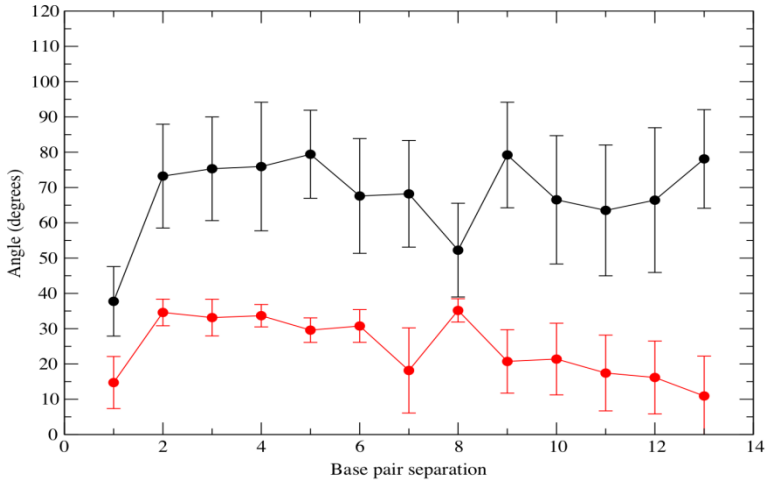

Figure 4-6. PA (black) and SA (red) twist angles with respect to the nearest DNA base pair.

flexibility of the system. To estimate the flexibility of the dyes compared to that of DNA, we computed the root mean square deviation (RMSD) with respect to the average structure (Figure

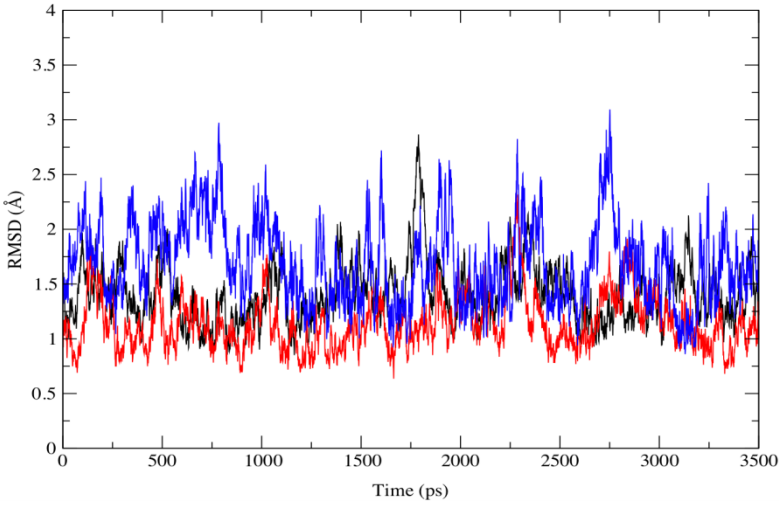

Figure 4-7. Heavy atom RMSD to average structure for system N = 12. All heavy atoms (black), 1.4 Å, DNA (red), 1.1 Å, and dyes (blue), 1.7 Å.

4-7) of the heavy atoms of DNA, dyes, and the entire system. The figure shows the RMSD of for N = 12 system. As can be seen in the figure, the RMSD of the probes, 1.7 Å, is slightly higher than that of the DNA, 1.3 Å. Both values, though, are within acceptable ranges of deviations for DNA MD simulations.[58, 62]

In Figure 4-8, we plot the orientation factor, κ^2, calculated from MD using the TDC method. Approximating θ_A and θ_D as 90°, based on our earlier measurements,

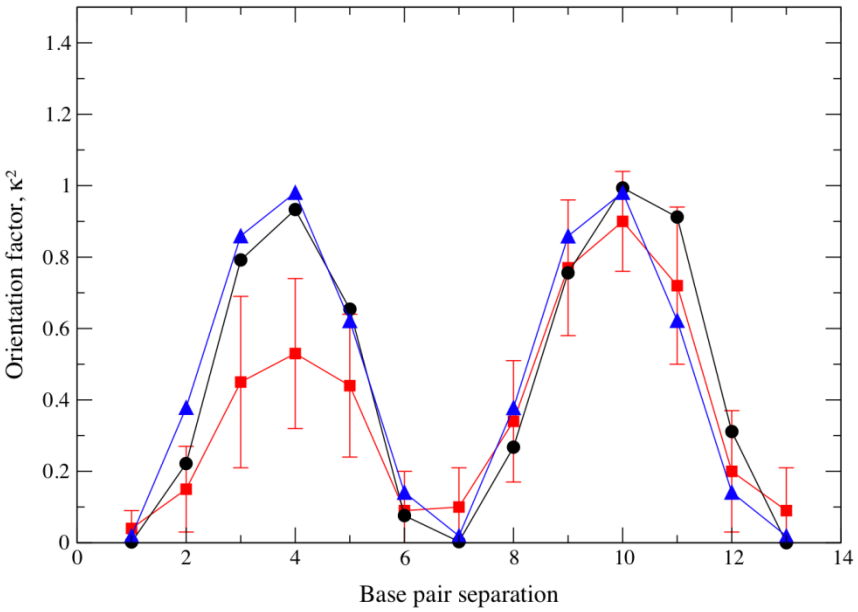

Figure 4-8. SA-PA orientation factor. Average κ^2 from MD (red) with standard deviation, $\cos^2(\theta_T)$ fit (black) and $\cos^2(68°+30°N)$ fit of the MD data (blue).

(Figure 4-5B), we are able to fit κ^2 as $\cos^2(\theta_T)$, where θ_T, in turn, can be approximated by the expression $68°+30°N$, where N is the number of base pairs. Note that the value of the orientation factor fluctuates between 0 and 1 corresponding to the two vectors perpendicular to the line between their centers and spanning orientations between perpendicular and parallel to each other, respectively. These results support the idea of using DNA as a scaffold for controlling dye separation and orientation as proposed by Lewis et al. If the exact values of the spectral overlap and donor's quantum yield are known, the value of R_0 could be adjusted for a specific donor-acceptor pair by varying the κ^2 value via changes in the base pair separation of the two probes. One drawback of such a procedure, however, is that at certain SA-PA orientations, κ^2 is near zero, which results in low energy transfer efficiencies even at very close separations. This means that in order for this procedure to be useful, twist angles of the dyes must be measured accurately to avoid labeling DNA at separations at which this can happen. Our values for the orientation

factor differ from those calculated by Lewis et al. (Figure 4-2C) mainly due to the differing estimates of the SA and PA twist angles.

In Figure 4-9 we examine the effect of the probe orientation on the rate of energy transfer. The figure presents a plot of FRET rates calculated using various approaches versus the number of base pairs. The first and second sets of values, k_{Coul} and $k_{dip\text{-}dip}$, were calculated based on V_{DA} couplings calculated with TDC using the full Coulombic potential and the dipole-dipole approximation, respectively. The third and fourth sets, $k_{För}$ (κ^2_{MD}) and $k_{För}$ ($\kappa^2_{2/3}$), were

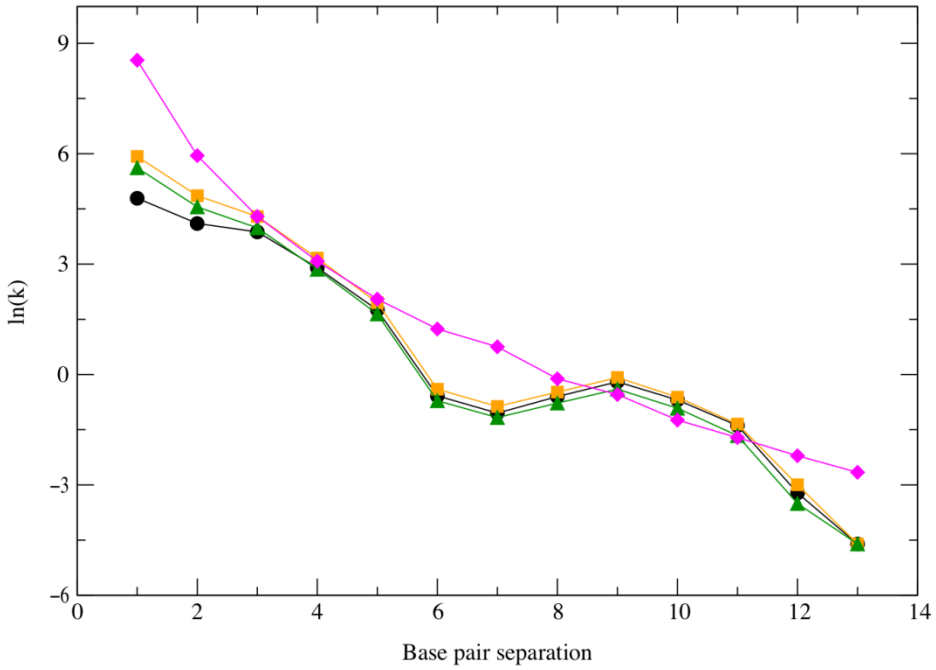

Figure 4-9. FRET rates for SA-PA pair at various base pair separations. TDC calculated k_{Coul} (black) and $k_{dip\text{-}dip}$ (green) and Förster calculated $k_{För}$, with κ^2 from MD (orange) and $\langle\kappa^2\rangle$ =2/3 (pink). Standard deviations are omitted for clarity.

calculated based on Förster theory, using $k = \tau_D^{-1}(R_0/R)^6$ where τ_D = 2.1 ns.[93] In the third set, both R and κ^2 were obtained from MD, while in the fourth set, $\langle\kappa^2\rangle$ = 2/3 was used. The rates were calculated for each frame and then averaged. As can be seen in the figure, for n = 1 to 2, i.e. at donor – acceptor separation of ~7 to 11 Å, the k_{Coul} rates are lower than the other sets of values. For these systems, the lengths of the donor and the acceptor, 5 Å, are significant in comparison to their separation and the dipole-dipole approximation at the basis of Förster is

invalid. Also, note that $k_{dip\text{-}dip}$ and $k_{För}$ (κ^2_{MD}) are in close agreement, which is expected since the two sets of values, though calculated with different approaches, are based on the same approximation of the dyes as point dipoles. The last set shows that use of the $<\kappa^2> = 2/3$ approximation results in completely erroneous rates. Most importantly, the wavelike decay of the rates, whether calculated using TDC or Förster theory, clearly demonstrates the orientational dependence of the FRET process.

In Figure 4-10, efficiencies calculated with molecular dynamics are compared to

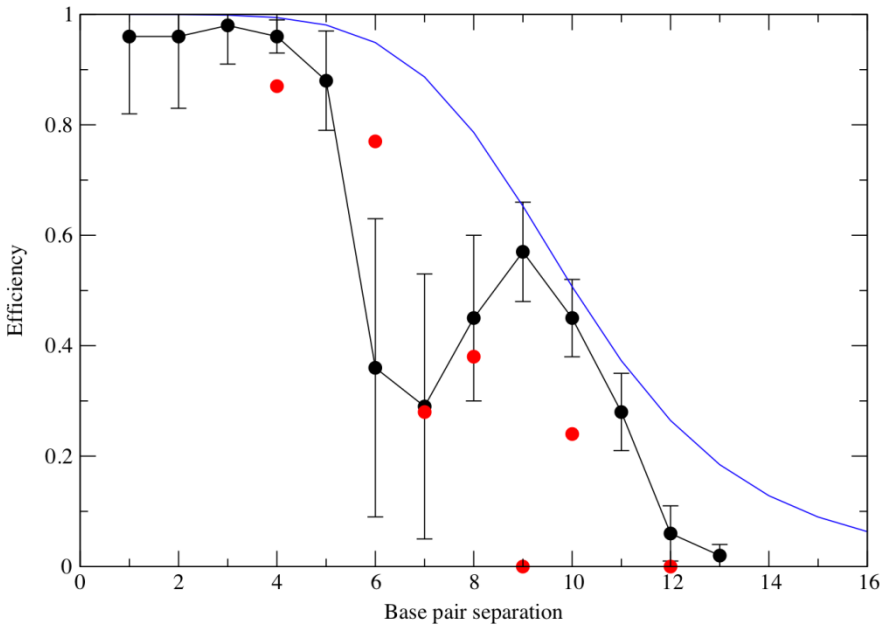

Figure 4-10. SA-PA efficiencies. MD data (black) with standard deviations, experimental data (red) and theoretical fit to $<\kappa^2> = 2/3$ (blue).

experimental values obtained using $E_{ff} = 1-\tau_{DA}/\tau_D$. As can be seen in the figure, MD values decay in a manner that reflects the helical nature of the DNA and is consistent with controlled orientation of the dyes. This trend is in a general agreement with the experimental results except for N = 9 system. We have to note that the experimental lifetime value of the donor in this case (and therefore the efficiency calculated based on it) are suspect, since the same efficiency calculated based on the donor quantum yield values provided in the same publication, is 0.27.

(E_{ff} = 1-Φ_{DA}/Φ_D where Φ_{DA} = 0.26 and , Φ_D = 0.35). Taking into consideration 15% estimated error in the experimental measurements, the agreement between our simulations and experiment becomes much more reasonable.

4.4 Conclusion

Lewis et al. suggested using DNA as a scaffold to control donor and acceptor orientations during the FRET process. Results of molecular dynamics simulations indicate that DNA does provide good control over both position and orientation of the probes with relatively little fluctuation in either. Orientation dependence of the rates and the efficiencies of energy transfer is demonstrated clearly by their wavelike mode of decay with distance. Our analysis indicates that applications of such systems are limited to cases in which the exact twist angle of the dyes is known in advance, so that donor/acceptor positions resulting in $\kappa^2 = 0$ can be avoided. Moreover, the system cannot be modeled with Förster theory at short donor-acceptor separations due to the breakdown of dipole-dipole approximation.

CHAPTER5
CYANINE DYES - DNA

5.1 Introduction

5.1.1 Background

Some of the oldest and most commonly used fluorescent probes belong to the cyanine dye family. The general structure of these dyes, as shown in Figure 5-1, includes a polymethine bridge between two nitrogen atoms with a delocalized positive charge.[71]

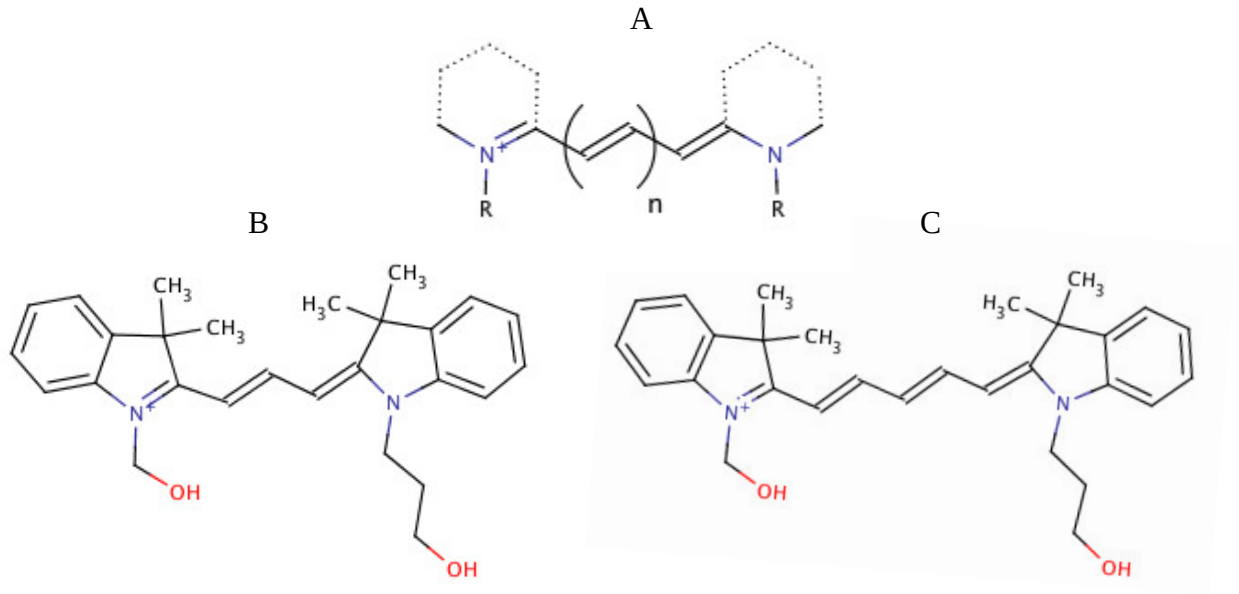

Figure 5-1. Cyanine dyes. A) Generic structure, where R is a side group and n is the number of methine groups. B) Cy3. C) Cy5.

Cy3 (*n*=3) and Cy5 (*n*=5) are two members of the family that are particularly popular in FRET experiments due to their stability against photobleaching, high absorption coefficient (> 10^5 M^{-1} cm^{-1}) and good quantum yield.[7] The Cy3 absorption and emission maxima are at 550 and 570 nm, respectively, while those of Cy5 are at 649 and 670 nm, respectively.[40] The two dyes have been used separately or as a donor/acceptor pair in a variety of DNA studies including

investigations of structural dynamics[104], protein-DNA interactions[105] and biosensor applications.[106]

Recently several reports have been published indicating that the photophysical behavior of the cyanine dyes is rather complex. Both Cy5[107] and Cy3[108] were found to undergo photoinduced isomerization in solution between fluorescent *trans* and dark *cis* states. In their ground state, the two dyes assume all-*trans* configurations.[107, 109] Upon the excitation of the ground *trans* state, several processes can happen[107]: 1) decay back to the *trans* ground state via fluorescence, k_f; 2) intersystem crossing to the lowest triplet state, k_{ISC}; 3) internal conversion, k_{IC}; and 4) *trans-cis* isomerization, k_{ISO}. Widengren and Schwille[107] estimated the rates of these processes for free Cy5 and Cy3 and for Cy5 attached to dsDNA. They found that the isomerization lifetime, τ_{ISO}, of Cy3 in water is about 14 ns while that of Cy5, slightly longer, about 40 ns. The intersystem crossing lifetimes were much longer for both dyes – on the order of 1 μs. When Cy5 was attached to a 24 base-pair DNA duplex, its isomerization lifetime increased by a factor of 4. The authors also estimated that due to the slow rate of thermal back-isomerization, almost 50% of Cy5 in solution exists in the *cis* state. The complexity of the photophysical properties of Cy3 is reflected in the dyes' multi-component fluorescence lifetime decay as illustrated in Table 5-1. As can be seen in the table, the Cy3 fluorescence lifetime increases upon attachment to DNA and becomes multiexponential. The numbers of lifetime components, their values, as well as their weights vary, however, significantly from study to study. Moreover, as the values obtained by Sanborn et al.[110] indicate, the lifetime properties also depend on whether Cy3 is attached to dsDNA, ssDNA or is bound internally to the DNA duplex.

Along with fluorescence lifetimes, Sanborn and co-workers measured rotational correlation times, τ_r, and quantum yields for a variety of Cy3-DNA complexes. Their

measurement of the anisotropy decay of Cy3 bound to ds- or ssDNA indicated the presence of fast and slow components of 0.2 and 2 ns, respectively, suggesting that Cy3 experiences two different environments with different rotational mobility. The authors also estimated the

Table 5-1. Fluorescence lifetimes of free and DNA-bound Cy3.

Study	Free Cy3 lifetime (ns)	DNA-bound Cy3 lifetime (ns)	Mode of attachment
Sabanayagam et al.[111]	0.15	0.22 (80%) 0.86 (20%)	dsDNA, internally labeled
Sanborn et al.[110]	0.18	0.29 (56%) 0.82 (44%)	dsDNA, 5'- end
Sanborn et al.	-	0.53 (51%) 2.0 (49%)	ssDNA, 5'- end
Sanborn et al.	-	0.24 (47%) 0.76 (39%)	dsDNA, internally labeled
Iqbal et al.[80]	-	1.04 (61.6%) 1.91 (21.4%) 0.39 (16.9%)	dsDNA, 5'- end
Malicka et al.[112]	-	1.36 (86%) 0.29 (14%)	dsDNA, 5'- end

activation energy of isomerisation. They found that the value is higher for Cy3 attached to ssDNA (33 kJ/mol) than it is when attached to dsDNA (27 kJ/mol), though both were higher than the value of freely diffusing Cy3 (19 kJ/mol). The quantum yield of the dye was also higher in the ssDNA complex (0.4) than in dsDNA and free Cy3, which both exhibited quantum yields of ~ 0.18.

Based on these findings, Sanborn et al. suggested a model in which the dyes exist in two main populations. In one, the dyes interact strongly with DNA, resulting in higher *trans-cis*

isomerization activation energy. In the other, the dye is free to rotate or interact weakly with the DNA, which reduces the *trans-cis* isomerization activation energy, and the quantum yield is reduced due to a higher occurrence of non-fluorescent *cis* isomer.

In a more recent study, Iqbal et al.[80] reported three components of fluorescent decay for Cy3 attached to dsDNA. They suggested the existence of several Cy3 populations, corresponding to Cy3 stacked on top of DNA in a manner similar to that of an additional base pair (τ_f =1.91 ns), some other mode of interaction with DNA (τ_f = 1.04 ns), and freely rotating Cy3 (τ_f = 0.39 ns). To explain these data, they fit their Cy3/Cy5 energy transfer efficiency measurements to a two-state model of Cy3 in which the dye spent some amount of time stacked on top of DNA with a side-to-side mobility, and about 30% of the time in an unstacked conformation. Interestingly, the fractional intensity of the longest lifetime, assigned to the dye stacked on top of DNA was only ~ 21%, with the remainder of the time spent in some other configuration.

5.1.2 Goals of the Study

Cyanine dyes possess many desirable properties as good donors and acceptors for FRET studies. However, their complex photophysical behavior depends strongly on their environment, the system and the mode of attachment. Molecular dynamics can provide valuable information about the manner of the interaction of these dyes with DNA and help to explain their various photophysical properties. This information could offer a starting point for improvement in experimental system design.

5.2 Cy3 - DNA

5.2.1 System and Methods

The system studied consisted of the Cy3-labeled double-stranded DNA considered in the experiments of Sanborn et al.[110] Cy3 was attached with a six-carbon tether to the 5'-end of a DNA strand with the following sequence: 5'-CTCTTCAGTTCAGCC-3'. A complementary sequence was used to generate the second part of the duplex. Cy3 partial atomic charges were obtained using the RESP charge-fitting method after optimizing its geometry with Hartree-Fock and a 6-31G* basis set in Gaussian. After initial minimization of the systems in implicit solvent (GB model), the probe was allowed to relax and sample different conformations for 2 ns by increasing the temperature to 400K and keeping DNA restrained with 30 kcal/mol$Å^2$ force constant. For this run, 10 frames at equally spaced intervals were selected and each served as a starting point for a new run subject to the following procedure. Each system was solvated in an octahedral solvent box of 5000 water molecules. The energy of the solvent and then the energy of the entire systems were minimized. Next, the system was equilibrated for 50 ps, while increasing the temperature from 0 to 300 K and the DNA was restrained with 10 kcal/mol$Å^2$ force constant. The entire system was then equilibrated with no restraints at constant pressure, for 100 ps. Production runs were implemented at constant volume with a 2 fs time step and durations of 36 to 43 ns. Results were saved every 1 ps. A total of 400 ns of simulation were performed. Trajectory frames were clustered using hierarchical clustering algorithm within *ptraj* module of AMBER package based on RMSD of Cy3 and adjacent base pair.

5.2.2 Results and Discussion

Hierarchical clustering of trajectory frames identified five predominant modes of Cy3-DNA interactions accounting for 73% of the total simulation time (Figure 5-2). Clusters A and B correspond to Cy3 stacking on top of DNA. In cluster A the 'free' indole ring of the dye interacts

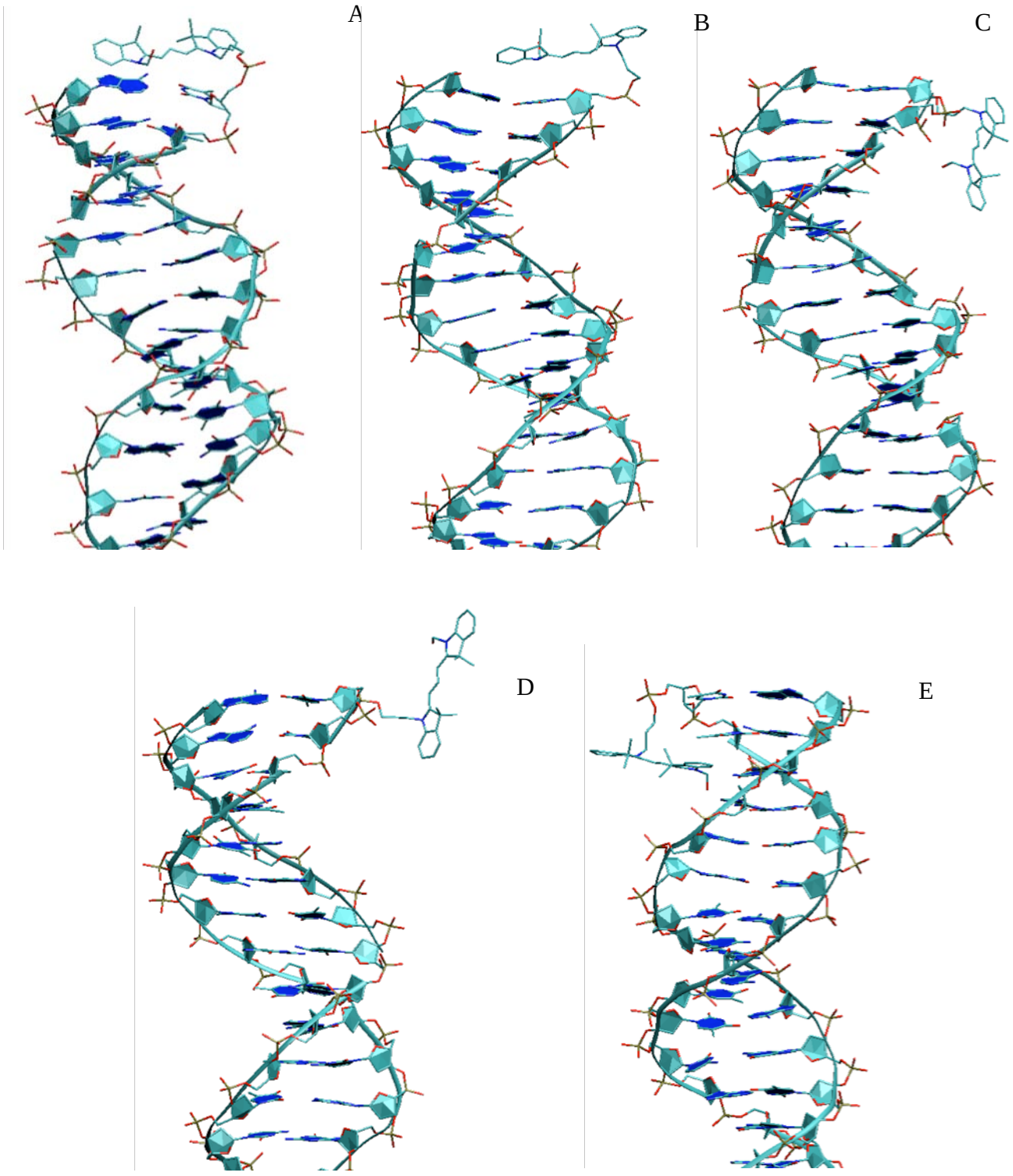

Figure 5-2. Representative structures of the five most populated Cy3-DNA clusters. A) 11.7%, B) 15.3 %, C) 19.6 %, D) 11.4%, and E) 14.9%.

primarily with the adenine ring of the opposite strand, while in cluster B the interaction between the 'free' indole Cy3 ring and the thymine of the same strand is predominant. This difference in stacking interactions appears to depend on which 'face' of Cy3 is closer to the DNA. Cluster C corresponds to a Cy3 position that fluctuates between freely rotating Cy3 and Cy3 interacting with the DNA through hydrogen-bonding and hydrophobic contacts. Cluster D represents freely rotating Cy3, and cluster E represents the Cy3 hydrogen bonding to the non-top base pairs as well as the backbone of the DNA. Visual analysis of the molecular dynamics showed that Cy3 exhibited interconversion between different conformations throughout the simulation time with the exception of the stacked conformation, in which, once assumed, the dye remained till the end of the simulation.

In order to estimate rotational freedom of various Cy3 conformations, we employed *ptraj* module of AMBER to calculate autocorrelation function for dipole vector of Cy3 assumed to lie along its long axis.[80] The angular correlation function[113] is defined as,

$$C_2(t) = \left\langle P_2\left[\mathbf{n}(0) \bullet \mathbf{n}(t)\right]\right\rangle \tag{5-1}$$

where $P_2(x)=1/2(3x^2-1)$ is the second-order Legendre polynomial and $\boldsymbol{n}$ is a vector rotating with the molecule. Thus, Cy3 correlation function was calculated for each system and converted to anisotropy *r(t)* using the following relationship,

$$r(t) = \frac{2}{5} C_2(t) \tag{5-2}$$

The computed anisotropy decays were fit the following expression,

$$r(t) = \sum_i r_{0i} \exp^{-t/\tau_{ri}} \tag{5-3}$$

where τ_{ri} are rotational correlation times of the fluorophore and r_{0i} are their fractional weights. The best fit was achieved with two correlation time values. Among the fitted parameters reported in Table 5-2, only τ_{r1} values have physical meaning. For example, throughout runs 4 and 8, Cy3

was observed to stack on top of DNA, which is reflected in its longer rotation correlation values of 5.7 and 6.8 ns, respectively. The other runs, where Cy3 fluctuated between free state and a state where in interacted with DNA through van der Waals and hydrogen bonding, exhibited a range of τ_{r1} from 0.7 ns to 2 ns most likely due to different amounts of time spent by Cy3 in free or DNA-bound state in each run. Direct comparison between simulation values and experiment is complicated by the fact that the diffusion coefficient for TIP3P water model - a property that has direct effect on rotational freedom of the solute - is significantly different from experimental values.[114] The presence of at least two distinctly different DNA-bound Cy3 rotational correlation times is in good agreement with Iqbal et al. findings. Note that in both experimental and MD anisotropy fittings, a short lifetime component is observed, however, it is our believe that it has no physical meaning.

Table 5-2. Cy3 rotation correlation times from MD.

Run	τ_1 (ns)	τ_2 (ns)
1	1.48	0.12
2	0.74	0.09
3	1.67	0.07
4	5.28	0.09
5	1.72	0.05
6	2.06	0.11
7	1.34	0.09
8	6.7	0.10
9	1.39	0.08
10	1.77	0.07

5.2.3 Conclusion

The results of our simulations indicated that Cy3 cyanine dye, when bound to 5'end of dsDNA, assumed several different conformations that have not been observed via NMR experiments performed by Norman et al. Specifically, aside from stacking on top of adjacent base pair as reported previously, the dye also exhibited freely rotating conformation as well as a state where it interacted with the backbone and non-top base pairs through hydrogen-bonding and wan der Waals forces. Fitting of anisotropy decay functions from MD simulations resulted in at least two distinct rotational correlation times corresponding to specific Cy3-DNA interaction modes and confirming experimental rotational correlation measurements of Iqbal et al.

5.3 Cy3/Cy5 - DNA

5.3.1 Experiment

Anisotropy measurements of many popular donors and acceptors attached to DNA indicate that the dyes do not rotate freely, despite the long flexible linkers used to attach them. Molecular dynamics studies described earlier in this work confirm these observations and demonstrate the various modes of interaction of the probes with DNA. The presence of these dye-DNA interactions introduces significant uncertainty in the interpretation of the FRET data if the $<\kappa^2>$ = 2/3 approximation is used in calculations of Förster radii. In an attempt to eliminate this uncertainty, Ranjit et al.[115] constructed a new type of system (Figure 5-3) in which Cy3 and Cy5 are attached to the backbone of the DNA in a manner that could provide control over the exact position and orientation of the dyes. The authors measured FRET efficiencies for three such dsDNA systems with donor-acceptor separations of 23, 26, and 29 base pairs (Table 5-1). The distances between the dyes were modeled based on the standard B-DNA geometry, and orientation factors were obtained from a fit of the experimental efficiencies.

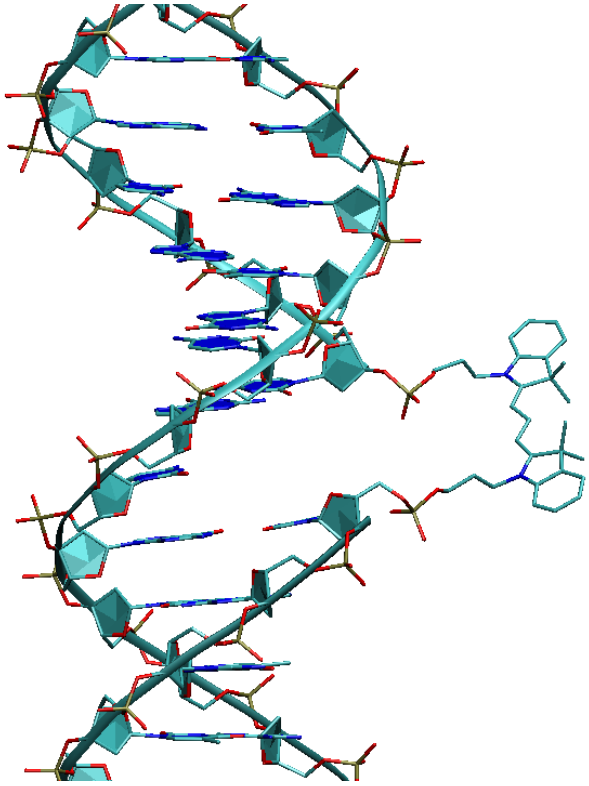

Figure 5-3. Backbone mode of attachment of Cy3 to DNA.

Table 5-3. Experimental Cy3/Cy5 efficiencies, modeled distances, and fitted κ^2 for N = 23, 26 and 29 systems. Data from Ranjit, et al. (unpublished)

N base pairs	Efficiency	R (Å)	κ^2
23	0.40	83	1.5
26	0.15	90	2.5
29	0.13	102	3.5

As can be seen in the table, the results suggested that DNA provides structural control over the position of the dipoles in a manner that results in κ^2 much larger than 2/3. Moreover, the value of κ^2 for $N = 29$ suggested that the dyes in this system are positioned more or less parallel to the long axis of the DNA and collinear to each other.

To investigate further the structural aspects of such system and to help explain the experimental findings, we performed molecular dynamics simulations of these dye-DNA complexes. We analyzed the interchromophore separation and the dye orientations and evaluated their effect on the efficiency of FRET.

5.3.2 System and Methods

The systems modeled consisted of double-stranded DNA complexes consisting of 60 base pairs, with Cy3 and Cy5 attached to the backbone phosphates through three-carbon tethers. For *N* = 23 and 26 the two probes were attached to the opposite strands with 23 and 26 base pairs between them, respectively, while for *N* = 29 the dyes were attached to the same strand. The following DNA sequences were used:

N = 23: 5'-GATGATGTCATCGACAGC-Cy3-
CGATATTAGCTCTCTAGCAGGGTAGCACAGGTGCGAGGCTG-3'
5'-CAGCCTCGCACCTGTGC-Cy5-ACCCTGCTAGAGAGCTAATATCGCGCTGTCGATG
ACATCATC-3'

N = 26:5'-GATGATGTCATCGAC-Cy3-
GCGCGATATTAGCTCTCTAGCAGGGTAGCACAGGTGCGAGGCTG-3'
5'-CAGCCTCGCACCTGTGC-Cy5-ACCCTGCTAGAGAGCTAATATCGCGCTGTCGATG
ACATCATC-3'

N = 29: 5'-GATGATGTCATCGAC-Cy3-GCGCGATATTAGCTCTCTAGCAGGGTAGC-
Cy5-CAGGTGCGAGGCTG-3'
5'-CAGCCTCGCACCTGTGCTACCCTGCTAGAGAGCTAATATCGCGCTGTCGATGACA
TCATC-3'

The charges on the dyes were assigned in the *antechamber* module of AMBER using the AM1-BCC model developed to reproduce RESP charges. Generalized Born implicit solvent

model was used to simulated electrostatic solvent effect. After initial minimization of the systems, the probes were allowed to relax and sample different conformations for 2 ns while increasing the temperature to 400K and keeping DNA restrained with 30 kcal/mol$Å^2$ force constant. From this run, 10 frames at equally spaced intervals were selected and each served as a starting point for a new run of 20 to 30 ns at 200 K. Trajectory frames were clustered using hierarchical clustering algorithm within *ptraj* module of AMBER package based on RMSD of Cy3 and adjacent base pair.

5.3.3 Results and Discussion

The results of the molecular dynamics indicated that both Cy3 and Cy5 assumed positions in which they interacted with DNA either in a minor groove or a major groove (Figure 5-4).

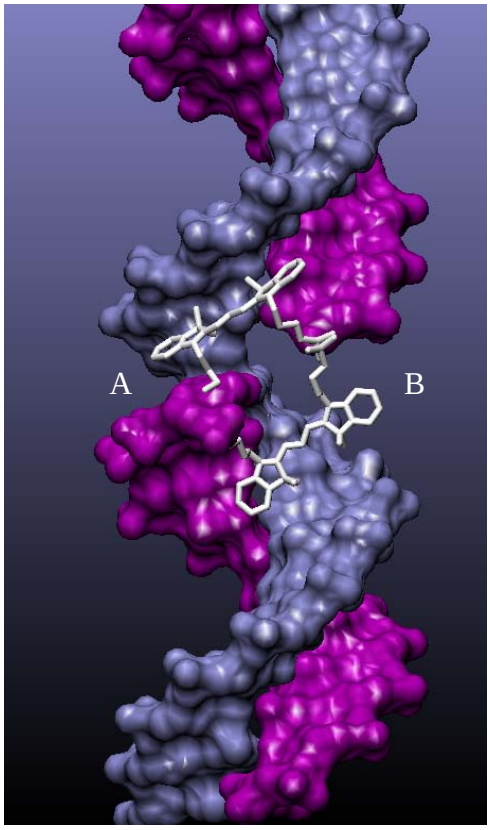

Figure 5-4. Modes of interaction of Cy3 with DNA. Overlay of two different runs for N = 23 system with DNA aligned. A) Minor groove. B) Major groove. Similar results were observed for Cy5.

Once the dyes moved into either position (usually within first 100 ps or so) they remained there throughout the remainder of the simulation, indicating that interaction with the DNA, most likely hydrophobic in nature, is much more favorable than remaining exposed to the polar solvent. We calculated theoretical energy transfer efficiencies for each system with the TDC method, using interchromophore distances and orientation factors from MD. The results, as shown in Figure 4-5, indicated the presence of three distinct sets of efficiencies clustered around different average distances. Visual analysis of the dynamics indicated that the different sets of distances

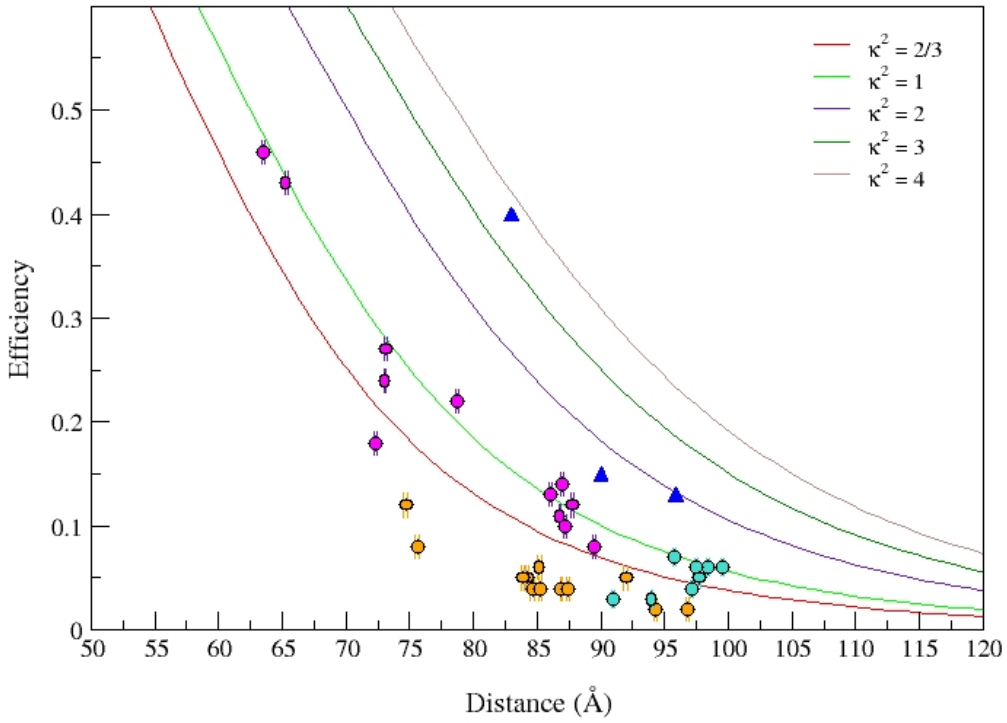

Figure 5-5. Average theoretical Förster efficiencies for the Cy3/Cy5 pair for each run for the N = 23 system (magenta), N = 26 (yellow) and N = 29 (blue-green), with the standard error included. Experimental efficiencies vs. distances calculated by Levitus et al. are depicted by blue triangles.

corresponded to different combinations of Cy3 and Cy5 binding modes, as shown in the cartoon in Figure 5-6. In fact, the average distance of each mode observed in MD can be fit with simple expressions (Table 5-2) for N = 23 and N = 26 systems. (N = 29 is discussed below). The

modeled distance for binding mode C is calculated differently for the two systems, because Cy3 partially intercalates in DNA while it binds in the minor groove in the $N = 26$ system.

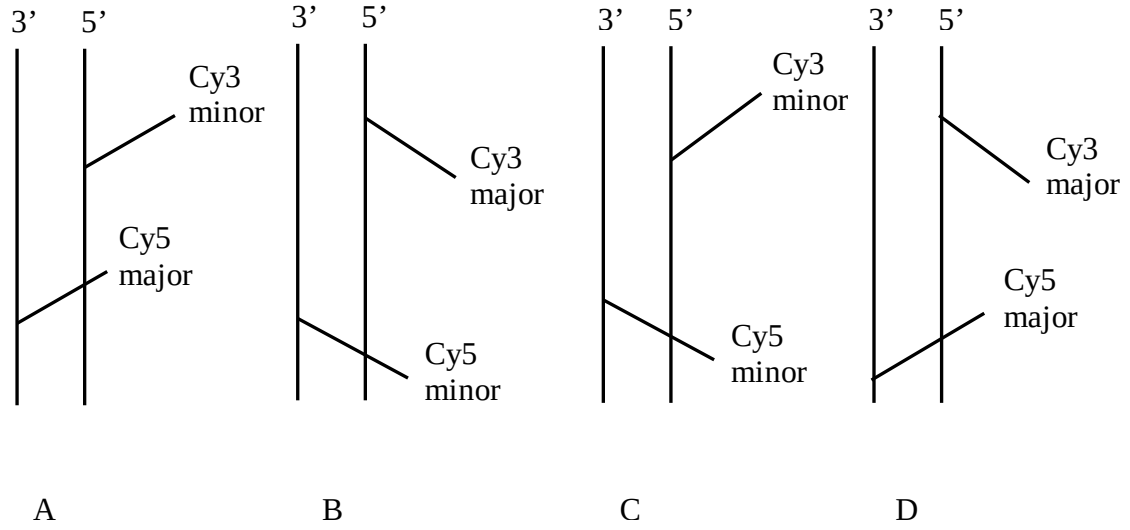

Figure 5-6. Different combinations of Cy3 and Cy5 binding modes.

Table 5-4. Modeled distances versus average MD distances for different Cy3/Cy5 binding modes. N is the number of base pairs and 3.4 Å is the standard base pair separation for B-DNA.[a] for N = 23. [b] for N = 26.

Mode	R_{mod}	N = 23		N = 26	
		R_{mod} (Å)	$\langle R \rangle_{MD}$ (Å)	R_{mod} (Å)	$\langle R \rangle_{MD}$ (Å)
A,B	(N-1)*3.4	74.8	74.3	85	85.4
C	[a]((N-1)+4)*3.4, [b]((N-1)+3)*3.4	88.4	87.4	95.2	94.3
D	((N-1)-4)*3.4	61.2	64.4	71.4	75.1

The DNA sequences surrounding the Cy3 location of attachment are different in the two systems, which supports the idea that cyanine dyes, while possessing qualities of both groove binders and intercalators, behave in the way that they do depending on the adjacent DNA sequence. The fact that experimental efficiency values are in the best agreement with theory for one mode of Cy3/Cy5 binding, specifically with both dyes bound in major grooves, indicates that

this mode is preferred, with binding in the minor groove occurring much less frequently. Notice that the average interchromophore distance for N = 23 systems is almost 20 Å shorter than the distance that is assumed using standard B-DNA geometry and 15 Å shorter for N = 26. An estimate of the fraction of time spent in any particular conformation for N = 23 can be made using the following expression,

$$\langle E_{ff} \rangle = a\langle E_{ff} \rangle_{A,B} + c\langle E_{ff} \rangle_{C} + d\langle E_{ff} \rangle_{D} \qquad (5\text{-}1)$$

where $\langle E_{ff} \rangle$ is the experimental efficiency value, and a, c, and d are the fractional weights of average efficiencies of each mode computed from MD, $\langle E_{ff} \rangle_{A,B}$, $\langle E_{ff} \rangle_{C}$ and $\langle E_{ff} \rangle_{D}$, respectively.

Table 5-5. Estimated fractional weight of each mode of Cy3-DNA binding for N = 23 system. A, c, and d are percent weight coefficients for $\langle E_{ff} \rangle_{A,B}$= 0.23, $\langle E_{ff} \rangle_{C}$= 0.11, and $\langle E_{ff} \rangle_{D}$= 0.45.

d (%)	a (%)	c (%)	$\langle E_{ff} \rangle$
80	10	10	0.39
80	15	5	0.4
80	5	15	0.39
70	25	5	0.38
70	30	0	0.38

The estimates in the table are rather crude, since the same quantum yield of 0.31 was used to calculate theoretical efficiencies for all modes, although this might not be necessarily true. As can be seen in the table, the Cy3/Cy5 spend at least 60% of the time bound in the major groove. Interestingly, the average κ^2 factors for each run of N = 23 system are all around ~ 0.90 value. Same trend is observed for N = 26 system, where κ^2 of each run are also similar and are ~ 0.30.

These results suggest that backbone attachment of the probes does provide some control of κ^2, though not in the manner expected.

The situation is rather different for the $N = 29$ system, where, though Cy3 and Cy5 also exhibit both major and minor groove binding, the dye-to-dye distances for each mode do not differ distinctly, and the average κ^2 value of each run varies from 0.39 to 1.0. The lack of consistency in these parameters suggests that this system allows more flexibility in the dye position and orientation, which might be related to the fact that both dyes are attached to the same strand.

5.3.4 Conclusion

The results of our simulations indicate that attachment of Cy3 and Cy5 dyes to the backbone of DNA, as proposed by Sanjit et al. provides control of the orientation factor κ^2 only in cases in which the two dyes are attached to opposite strands. This mode of attachment results in binding of dyes in either a major groove or a minor groove, and significant interchromophore variation in distance of up to 20 Å depending on the dye-DNA interaction mode. Experimental results are in excellent agreement with theory in cases in which both dyes bind in the nearest major groove, suggesting that other modes of interaction are insignificant on the time scale of the experiment. The interchromophore distance for this case can be estimated by the expression (N-5)*3.4, where N is the number of base pairs between the dyes.

CHAPTER 6
CONCLUSIONS

Among the many available single-molecule fluorescence techniques, single-molecule resonance energy transfer (smFRET) is one of the most popular and widely used largely due to high sensitivity of the fluorescent emission to the orientation and location of the molecule and environmental factors. The technique is particularly important for biological systems in solution, for which direct structural information is difficult to obtain. The process of resonance energy transfer is based on the ability of an electronically excited fluorescent molecule (the donor) to transfer energy through space to a second molecule (acceptor) with an efficiency that is defined by Förster theory to depend on the donor-acceptor distance raised to the negative power of six. In FRET experiments, measured efficiency is used to infer interdye distance and, hence, dynamic and structural changes in a system. Thus, FRET has been used to investigate, among other processes, conformational dynamics of Holliday junctions, folding states of ribozyme hairpin, DNA melting, and DNA-cofactor interactions in which relative distance changes were correlated to interconversion between various states of the systems. Measuring relative rather than absolute distances remains a standard approach in FRET experiments even at a single-molecule level due to lack of knowledge about the probe position and orientation with respect to each other and the system. The long linkers through which the dyes are attached to DNA, the large size of the probes themselves, as well as the possibility of their interaction with the system add to this uncertainty.

In this work we described molecular dynamics studies of several dye-DNA systems in which we examined how fluorescent probes interact with DNA and the effects of these interactions on FRET. Our study of a Cy5-TMR-labeled DNA system showed that both dyes interact with DNA and assume multiple conformations that interconvert on the time-scale of the

experiment. As a general trend, the average donor-acceptor distances were smaller than the values predicted using standard B-DNA model. This discrepancy, which for some systems was as high as 10 Å, was caused primarily by the presence of two different positions assumed by Cy5 with respect to DNA. Cy5 interconversion between two conformations also caused large fluctuations in both the interchromophore distance and the orientation factor, which resulted in a broad distribution of experimental efficiencies. An analysis of the orientation factor averages and distributions indicated that the static, rather than the dynamic, limit of efficiency averaging is the correct approach for this particular system.

In the second study, we investigated use of DNA as a scaffold to control donor and acceptor orientations during the FRET process as proposed by Lewis et al. Results of molecular dynamics simulations indicated that DNA provided good control over both position and orientation of the probes attached at the opposite ends of DNA in a manner of additional base pairs. In addition, we demonstrated orientational dependence of the rates and the efficiencies of energy transfer that decayed in a wavelike manner with distance. Our analysis indicated that applications of such systems are limited to cases in which the exact twist angle of the dyes is known in advance, so that donor/acceptor positions resulting in $\kappa^2 = 0$ can be avoided. Moreover, we demonstrated that the system could not be modeled with Förster theory at short donor-acceptor separations due to the breakdown of dipole-dipole approximation.

In out next study, we conducted simulations of dsDNA-bound Cy3 cyanine dye. The results indicated that the dye, expected to stack on top of DNA based on NMR studies, in fact, fluctuated between several conformations. Specifically, aside from stacking on top of the adjacent base pair, the dye also exhibited freely rotating conformation as well as a state where it interacted with the backbone and non-top base pairs through hydrogen bonding and van der

Waals forces. Fitting of anisotropy decay functions from MD simulations resulted in at least two distinct rotational correlation times corresponding to specific Cy3-DNA interaction modes and confirming experimental rotational correlation measurements.

The results of last study indicated that attachment of Cy3 and Cy5 dyes to the backbone of DNA, as proposed by Sanjit et al. provides control of the orientation factor κ^2 only in cases in which the two dyes are attached to opposite strands. This mode of attachment resulted in binding of dyes in either a major groove or a minor groove, and significant interchromophore variation in distance of up to 20 Å depending on the dye-DNA interaction mode. Experimental results were in excellent agreement with theory in cases in which both dyes bound in the nearest major groove, suggesting that other modes of interaction were insignificant on the time scale of the experiment. The interchromophore distance for this case was estimated by the expression (N-5)*3.4, where *N* is the number of base pairs between the dyes.

The above findings can be used to make general suggestions about probe position and mode of attachment to DNA that will allow more accurate FRET distance measurements. First, since long linkers do not provide rotational freedom of the probes as originally intended, but instead allow dyes to interact with different parts of DNA causing large uncertainty in distance measurements, shorter tethers should be used. Based on Cy5/TMR-DNA and Cy3/DNA studies, it is reasonable to conclude that unless a probe possesses large negative charge, it most likely will interact with DNA whether its tether is long or short. Therefore, attempt to guarantee free rotation of the dyes through long linkers is futile and unnecessary considering that the overall rotation of DNA (ns) will result in random reorientation of the probes' dipole moments in between detection of consecutive photon (μs).

Our other conclusion is that attachment of the probes at opposite ends of dsDNA in a manner of additional base pairs will allow for excellent control over the dyes' separation and orientation. For this design to be useful, however, the exact twist angle of the dyes with respect to their adjacent base pairs has to be determined (either through experimental measurement or modeling) to avoid donor-acceptor separations where this angle is a multiple of $\pi/2$ in which case $\kappa^2 = 0$ and no transfer takes place. This system design can be extended to other fluorophores. In fact, covalent attachment of Cy3 to both strands of DNA in a manner similar to stilbene fluorophore would resolve the problem of multiple Cy3 conformation and allow for better control over its position and orientation.

Finally, backbone attachment of the probes can be a useful system design as well, with few modifications to the original approach. While the results of our simulations indicated that cyanine dyes prefer to bind into major groove, the reason for this preference is not clear and could be equally attributed to dye-DNA interaction specific to cyanine dyes, or to the sequence of DNA, or both. This makes prediction of the groove-binding preference (and therefore exact donor-acceptor separation) for any other probes/DNA sequences rather difficult. One way to avoid this problem could be by using probes with large negative charge, which would cause the dyes to be repelled by the DNA backbone and remain exposed to the polar solvent. Standard B-DNA geometry and minimal modeling can then be used to compute both orientation and separation of the probes.

LIST OF REFERENCES

1. Lakowicz, J. R. 1999. Principles of Fluorescence Spectroscopy. Kluwer Academics/Plenum Publishers, New York.

2. Reviews in Fluorescence. 2004. Geddes, C.D., Lakowicz, J. R., eds. Kluwer Academics/Plenum Publishers, New York.

3. Weiss, S. 1999. Fluorescence spectroscopy of single biomolecules. *Science*. 283:1676-1683.

4. Selvin, P. R. 2000. The renaissance of fluorescence resonance energy transfer. *Nat. Struct. Biol*. 7:730-734.

5. Deniz, A. A., S. Mukhopadhyay, and E. A. Lemke. 2007. Single-molecule biophysics: at the interface of biology, physics and chemistry. *J. R. Soc. Interface*. 5:15-45.

6. Roy, R., S. Hohng, and T. Ha. 2008. A practical guide to single-molecule FRET. *Nat. Methods*. 5:507-516.

7. Joo, C., H. Balci, Y. Ishitsuka, C. Buranachai, T. Ha. 2008. Advances in single-molecule fluorescence methods for molecular biology. *Ann. Rev. Biochem*. 77:51-76.

8. Yildiz, A., J. N. Forkey, S. A. McKinney, T. Ha, Y. E. Coldman, and P. R. Selvin. 2003. *Science*. Myosin V walks hand-over-hand: single fluorophore imaging with 1.5 nm localization. 300: 2061-2065.

9. Talaga, D. S., W. L. Lau, H. Roder, J. Y. Tang, Y. W. Jia, W. F. DeGrado, and R. M. Hochstrasser. 2000. Dynamics and folding fo single two-stranded coiled-coil peptides studied by fluorescent energy transfer confocal microscopy. *Proc. Natl. Acad. Sci. USA*. 97:13021-13026.

10. Ying, L. M., J. J. Green, H. T. Li, D. Klenerman, and S. Balasubramanian. 2003. Studies on the structure and dynamics of the human telomeric G quadruplex by sinlge-molecule fluorescence resonance energy tranfsre. *Proc. Natl. Acad. Sci. USA.* 100:14629-14634.

11. Yu, J., J. Xiao, X. J. Ren, K. Q. Lao, and X. S. Xie. 2006. Probing gene expression in life cells, one protein molecule at a time. *Science*. 311:1600-1603.

12. Dickerson, R. E., H. R. Drew, B. N. Conner, R. M. Wing, A. V. Fratini, M. L. Kopka. 1982. The anatomy of A-, B-, and Z-DNA. *Science*. 216:475-485

13. Perrin, F. 1932. Théorie quantique des transferts d'activation entre molécules de même espece. Cas des solutions fluorescentes. *Ann. Phys*. 17:283-314.

14. Förster, T. 1946. Energy migration and fluorescence. *Naturwiss*. 33:166-175.

15. Förster, T. 1948. Intermolecular energy transference and fluorescence. *Ann. Physik*. 2:55-75.

16. Förster, T. 1965. Delocalized excitation and excitation transfer. *In* Modern Quantum Chemistry. O. Sinanoglu, editor. Academic Press, Inc., New York.

17. van der Meer, B. W., G. I. Coker, and S.-Y. Chen. 1994. *In* Resonance Energy Transfer: Theory and Data. VCH Publishers, New York.

18. Haugland, R. P., J. Yguerabide, and L. Stryer. 1969. Dependence of the kinetics of singlet-singlet energy transfer on spectral overlap. *Proc. Natl. Acad. Sci. USA.* 63:23–30.

19. Hillel, Z. C.-W., Wu. 1976. Statistical interpretation of fluorescence energy transfer measurements in macromolecular systems. *Biochem*. 15:2105-2113.

20. Stryer, L. 1978. Fluorescence energy transfer as a spectroscopic ruler. *Annu. Rev. Biochem.* 47:819–846.

21. Stryer, L., and R. P. Haugland. 1967. Energy transfer: a spectroscopic ruler. *Proc. Natl. Acad. Sci. USA.* 58:719–726.

22. Vanderkooi, J. M., A., Ierokomas, H. Nakamura, and A. Martonosi. 1972. Fluorescence energy transfer between Ca^{2+} transport ATPase molecules in artificial membranes. *Biochem*. 16:1262-1267.

23. Wu, C.-W., L. Stryer. 1972. Proximity relationships in rhodopsin. *Proc. Natl. Acad. Sci. USA.* 69:1104-1108.

24. Schuler, B., E. A. Lipman, W. A. Eaton. 2002. Probing the free energy surface for protein folding with single molecule fluorescence spectroscopy. *Nature*. 419:743-747.

25. Scholes, G. D. 2003. Long range resonance energy transfer in molecular systems. *Annu. Rev. Phys. Chem*. 54:57-87.

26. Clegg R. M., A. I. H. Murchie, A. Zechel, and D. M. J. Lilley. 1993. Observing the helical geometry of double-stranded DNA in solution by fluorescence resonance energy transfer. *Proc Natl Acad Sci USA.* 90:2994–2998.

27. Jia, Y., D. S. Talaga, W. L. Lau, H. S. M. Lu, W. F. DeGrado and R. M. Hochstrasser. 1999. Folding dynamics of single GCN-4 peptides by fluorescence resonant energy transfer confocal microscopy. *Chem. Phys*. 247: 69-83.

28. Kulzer, F., and M. Orrit. 2004. Single-molecule optics. *Ann. Rev. Phys. Chem.* 55: 585-611.

29. Deniz, A. A., M. Dahan, J. R. Grunwell, T. Ha, A. E. Faulhaber, D. S. Chemla, S. Weiss, and P. G. Schultz. 1999. Sinlge-pair fluorescence resonance energy transfer on freely

diffusing molecules: Observation of Forster distance dependence and subpopulations. *Proc. Natl. Acad. Sci. USA* 96:3670-3675.

30. Deniz, A. A., T. A. Laurence, G. S. Beligere, M. Dahan, A. B. Martin, D. S. Chemla, P. E. Dawson, P. G. Schultz, and S. Weiss. 2000. Single-molecule protein folding: Diffusion fluorescence resonance energy transfer studies of the denaturation of chymotrypsin inhibitor 2. *Proc. Natl. Acad. Sci. USA*. 97:5179- 5184.

31. Ha, T., T. Enderle, D. F. Ogletree, D. S. Chemla, P. R. Selvin and S. Weiss. 1996. Probing the interaction between two single molecules: Fluorescence resonance energy transfer between a single donor and a single acceptor. *Proc. Natl. Acad. Sci. USA*. 93:6264-6268.

32. Ha, T., A. Y. Ting, J. Liang, W. B. Caldwell, A. A. Deniz, D. S. Chemla, P. G. Schultz, and S. Weiss. 1999. Single-molecule fluorescence spectroscopy of enzyme conformational dynamics and cleavage mechanism. *Proc. Natl. Acad. Sci. USA*. 96:893-898.

33. Rhoades, E., E. Gussakovsky, and G. Haran. 2003. Watching proteins fold one molecule at a time. *Proc. Natl. Acad. Sci. USA*. 100:3197-3202.

34. Merchant, K. A., R. B. Best, J. M. Louis, I. V. Gopich, W. A. Eaton. 2007. Characterization the unfolded states of proteins using single-molecule FRET spectroscopy and molecular simulations. *Proc. Natl. Acad. Sci. USA*. 104:1528-1533.

35. van der Meer, B. W. 1999. *In* Resonance Energy Transfer. John Wiley & Sons, Inc., New York.

36. O'Connor, D. V., and D. Phillips. 1984. Time-correlated single photon counting. Academic Press, New York.

37. Deniz A. A., T. A. Laurence, M. Dahan, D. S. Chemla, P. T. Schultz, S. Weiss. 2001. Ratiometric single-molecule studies of freely diffusing biomolecules. *Ann. Rev. Phys. Chem.* 52:233-253.

38. Rosenberg, S. A., M. E. Quinlan, J. N. Forkey, and Y. E. Goldman. 2005. Rotational motions of macro-molecules by single-molecule fluorescence microscopy. *Acc. Chem. Res.* 38:5883-593.

39. Nishizaka, T., K. Oiwa, H. Noji, S. Kumar, E. Muneyuki, M. Yoshida, and K. Kinosita Jr. 2004. Chemomechanical coupling in F1-ATPase revealed by simultaneous observation of nucleotide kinetics and rotation. *Nat. Struct. Biol.* 11:142-148.

40. Mujumdar, R. B., L. A. Ernst, S. R. Mujumdar, C. J. Lewis, and A. S. Waggoner. 1993. Cyanine dye labeling reagents: sulfoindocyanine succinimidyl esters. *Bioconj. Chem.* 4:105-111.

41. Ha, T. 2001. Single-molecule fluorescence resonance energy transfer. *Methods*. 25:78-86.

42. Gopich, I. V., and A. Szabo. 2005. Theory of photon statistics in single-molecule Forster resonance energy transfer. *J. Chem. Phys.*122:014707-1-014707-18.

43. Dahan M., A. Deniz, T. Ha, D. Chemla, P. Schultz, S. Weiss. 1999 Ratiometric measurement and identification of single diffusing molecules. *Chem. Phys*. 247: 85-106

44. Gopich, I. V., and A. Szabo. 2007. Single-molecule FRET with diffusion and conformational dynamics. *J. Phys. Chem. B.* 111:12925-12932.

45. Geva, E., and J. L. Skinner. 1998. Two-state dynamics of single biomolecules in solution. *Chem. Phys. Lett.* 288: 225-229.

46. Clegg, R. M. 1992. Fluorescence resonance energy transfer and nucleic acids. *Methods Enzym*. 211:353-388.

47. Ha, T. 2001. Single-molecule fluorescence methods for the study of nucleic acids. *Curr. Opin. Struct. Biol.* 11:287-292.

48. McKinney, S. A., A.-C. Déclais, D. M. J. Lilley, and T. Ha. 2002. Structural dynamics of individual Holliday junctions. *Nat. Struct. Biol.* 10:93-97.

49. Tan, E., T. J. Wilson, M. K. Nahas, R. M. Clegg, D. M. J. Lilley, and T. Ha. 2003. A four-way junction accelerates hairpin ribozyme folding via a descrete intermediate. *Proc. Natl. Acad. Sci. USA*. 100:9308-9313.

50. Li, H. T., X. J. Ren, L. M. Ying, S. Balasubramanian, and D. Klenerman. 2004. Measuring single-molecule nucleic acid dynamics in solution by two –color filtered ratiometric fluorescence correlation spectroscopy. *Proc. Natl. Acad. Sci. USA.* 101:14425-14430.

51. Lee, T.-H., L. J. Lapidus, W. Zhao, K. J. Travers, D. Herschlag, and S. Chu. 2007. Measuring the folding transition time of single RNA molecules. *Biophys. J.* 92:3275-3283.

52. Leger, J. F., J. Robert, L. Bourdieu, D. Chatenay, and J. F. Marko. 1998. RecA binding to a single double-stranded DNA moelcule: a possible role of DNA conformational fluctuations. *Proc. Natl. Acad. Sci. USA.* 95:12295-12299.

53. Case, D. A.,T. A. Darden, T. E. Cheatham III, C. L. Simmerling, J. Wang, R. E. Duke, R. Luo, K. M. Merz, D. A. Pearlman, M. Crowley, R. C. Walker, W. Zhang, B. Wang, S. Hayik, A. Roitberg, G. Seabra, K. F. Wong, F. Paesani, X. Wu, S. Brozell, V. Tsui, H. Gohlke, L. Yang, C. Tan, J. Mongan, V. Hornak, G. Cui, P. Beroza, D. H. Mathews, C. Schafmeister, W. S. Ross and P. A. Kollman. 2006. AMBER 9, University of California, San Francisco.

54. Cramer, C. J. 2002. Essentials of Computational Chemistry. Theories and Methods. John Wiley and Sons, Ltd., West Susssex, England.

55. Wang, J., P. Cieplak and P. A. Kollman. 2000. How well does a restrained electrostatic potential (RESP) model perform in calculating conformational energies of organic and biological molecules?. *J. Comput. Chem.* 21**:**1049-1074.

56. Wang, J., R. M. Wolf, J. W. Caldwell, P. A. Kollamn and D. A. Case. 2004. Development and testing of a general Amber forcefield. *J. Comput. Chem.* 25: 1157-1174.

57. Hawkins, G. D., C. J. Cramer and D. G. Truhlar. 1995. Pairwise solute descreening of solute charges from a dielectric medium. *Chem. Phys. Lett.* 246:122–129.

58. Tsui V., and D. A. Case. 2000. Molecular dynamics simulations of nucleic acids with a generalized born solvation model, *J. Am. Chem. Soc.* 122:2489–2498.

59. Bashford D., and D. A. Case. 2000. Generalized Born models of macromolecular solvation effects. *Ann. Rev. Phys. Chem.* 51:129-152.

60. Tsui, V., and D. Case. 2001. Theory and applications of the generalized Born solvation model in macromolecular simulations. *Biopolymers*. 5:275-291.

61. Izaguirre, J. A., D. P. Catarello, J. M. Wozniak and R. D. Skeel. 2001. Langevin stabilization of molecular dynamics. *J. Chem. Phys.* 114**:**2090-2098.

62. Cui, G. and C. Simmerling. 2002. Conformational heterogeneity observed in simulations of a pyrene-substituted DNA. *J. Am. Chem. Soc.* 124:12154-12164.

63. Krueger, B. P., G. D. Scholes, R. Jimenez, G. R. Fleming. 1998. Electronic excitation transfer from carotenoid to bacteriochlorophyll in the purple bacterium *Rhodopseudomonas acidophila*. *J. Phys. Chem. B* 102:2284-2292.

64. Scholes, G. D. 1999. Resonance Energy Transfer. John Wiley & Sons, Inc., New York.

65. Krueger, B. P., G. D. Scholes, G. R. Fleming. 1998. Calculation of couplings and energy-transfer pathways between the pigments of LH2 by the ab initio transition density cube method. *J. Phys. Chem. B* 102:5378-5368.

66. Head-Gordon et al. 2006. Advances in quantum chemical methods and algorithms in the Q-Chem 3.0 program package. Phys. Chem. Chem. Phys., 8, 3172

67. Dolghih, E., A. E. Roitberg, and J. L. Krause. 2007. Fluorescence resonance energy transfer in dye-labeled DNA. *J. Photochem. Photobiol A*. 190:321-327.

68. Dolghih, E., W. Ortiz, S. Kim, B. P. Krueger, J. L. Krause, A. E. Roitberg. (submitted) Theoretical studies of short polyproline systems: recalibration of a molecular ruler. J. Phys. Chem.

69. Neidle, S. 2001. DNA minor-groove recognition by small molecules. *Nat. Prod. Rep.* 18:291-309.

70. Strekowski, L., and B. Wilson. 2007. Noncovalent interactions with DNA: an overview. *Mutat. Res.* 623:3-13.

71. Armitage, B. A. 2005. Cyanine-dye-DNA interactions: intercalation, groove binding, and aggregation. *Top. Curr. Chem.* 253:55-76.

72. Guan, U., R. Shi, X. Li, M. Zhao, Y. Li. 2007. Multiple binding modes for dicationic Hoescht 33258 to DNA. J. Phys. Chem. B. 11:7336-7344.

73. Vámosi, G., C. Gohlke, and R. M. Clegg. 1996. Fluorescence characteristics of 5-carboxytetramethylrhodamine linked covalently to the 5' end of oligonucleotides: multiple conformers of single-stranded and double-stranded dye-DNA complexes. *Biophys. J.* 71:972-994

74. Eggeling, C., J. R. Freis, L. Brand, R. Günther, and C. A. M. Seidel. 1998. Monitoring conformational dyanmics of a single molecule by selective fluorescence spectroscopy. *Proc. Natl. Acad. Sci. USA.* 95:1556-1561.

75. Dietrich, A., V. Buschmann, C. Müller, M. Sauer. 2002. Fluorescence resonance enrgy transfer (FRET) and competing processes in donor-acceptor substituted DNA strands: a comparative study of ensemble and single-molecule data. *Rev. Mol. Biotech.* 82: 211-231.

76. Wang, L., A. K. Gaigalas, J. Blasic, and M. J. Holden. 2004. Spectroscopic characterization of fluorescein- and tetramethylrhodamine-labeled oligonucleotides and their complexes with a DNA template. Spectrochim. Acta A. 60:2741-2750.

77. Unruh, J. R., G. Gokulrangan, G. H. Lushington, C. K. Johnson, and G. S. Wilson. 2005. Orientational dynamics and dye-DNA interactions in a dye-labeled DNA aptamer. *Biophys. J.* 88:3455-3465.

78. Norman, D. G., R. J. Grainger, D. Uhrín, and D. M. J. Lilley. 2000. Location of cyanine-3 on double-stranded DNA: importance for fluorescence resonance energy transfer studies. *Biochem.* 39:6317-6324.

79. Iqbal, A., L. Wang, K. C. Thompson, D. M. J. Lilley, and D. G. Norman. 2008. The structure of Cyanine 5 terminally attached to double-stranded DNA: implications for FRET studies. *Biochem.* 47:7857-7862.

80. Iqbal, A., S. Arslan, B. Okumus, T. J. Wilson, G. Giraud, D. G. Norman, T. Ha, and D. M. J. Lilley. 2008. Orientation dependence in fluorescent energy transfer between Cy3 and Cy5 terminally attached to double-stranded nucleic acids. *Proc. Natl. Acad. Sci. USA* 105:11176-11181.

81. Lorenz M., A. Hillisch, S. D. Goodman, and S. Diekmann. 1999. Global structure similarities of intact and nicked DNA complexed with IHF measured in solution by fluorescence resonance energy transfer. *Nucleic. Acids Res.* 27:4619-4625.

82. Zimmerman, B., M. Diez, N. Zarrabi, P. Gräber, and M. Börsch. Movement of the ε-subunit during catalysis and activation in single membrane-bound h+atp. Eur Mol. Biol. Org. 24 (2005) 2053-2063.

83. Lee, N. K., A. N. Kapanidis, Y. Wang, X. Michalet, J. Mukhopadhyay, R. H. Ebright, and S. Weiss. Accurate FRET measurements within single diffusing biomolecules using alternating-laser excitation, Biophys. J. 88 (2005) 2939-2953.

84. Schobel, U., H.-J. Egelhaaf, A. Brecht, D. Oelkrug, and G. Gauglitz. New donor-acceptor pair for fluorescent immunoassays by energy transfer. Bioconjug. Chem. 10. 1999. 1107-1114.

85. Dale, R. E., and J. Eisinger. 1976 Intramolecular energy transfer and molecular conformation. Proc. Natl. Acad. Sci. USA 73:271-273.

86. Dale, R. E., J. Eisinger, and W. E. Blumberg. 1979. The Orientational freedom of molecular probes. *Biophys. J.* 26:161-194

87. Saito, K., T. Aoki, and T. Yanagida. 1994. Movement of single myosin filaments and myosin step size on an actin filament suspsended in solution by a laster trap. *Biophys. J.* 66:769-777.

88. Dos Remedios, C. G., and P. D. J. Moens. 1995. Fluorescence resonance energy tranfser spectrsoscopy is a reliable "ruler" for measuring structural changes in proteins. *J. Struct. Biol*. 115:175-185.

89. Wong, K. F., B. Bagchi, and P. J. Rossky. 2004. Distance and orientation dependence of excitation transfer rates in conjugated systems: beyond the Forster theory. *J. Phys. Chem. A* 108:5752-5763.

90. Ortiz, W., B. P. Krueger, V. D. Kleimna, J. L. Krause, and A. E. Roitberg. 2005. Energy transfer in the nanostar: the role of Coulombic coupling and dynamics. *J. Phys. Chem. B* 109:11512-11519.

91. Khan, Y. R., T. E. Dykstra, G. D. Scholes. 2008. Exploring and Forster limit in a small FRET pair. *Chem. Phys. Lett*. 461:305-309.

92. VanBeek, D. B., M. C. Zwier, J. M. Short, and B. P. Krueger. 2007. Fretting about FRET: correlation between κ and R. *Biophys. J.* 92:4168-4178.

93. Lewis, F. D., L. Zhang, and X. Zuo. 2005. Orientational control of fluorescence resonance energy transfer using DNA as a helical scaffold. *J. Am. Chem. Soc.* 127:10002-10003.

94. Lewis, F.D., X. Liu, Y. Wu, S. E. Miller, M. R. Wasielewski, R.L. Letsinger, R, R. Sanishvili, A. joachimiak, V. Tereshhko, and M. J. Egli. J. Am. Chem. Soc. 1999. 121. 9905-9906.

95. Lewis, F. D., L. Zhang, X. Liu, X. Zuo, D. M. Tiede, H. Long, G. C. Schatz. 2005. DNA as a helical ruler: exciton-coupled circular dichroism in DNA conjugates. J. Am. Chem. Soc. 127:14445-14453.

96. Letsinger, R. L., and T. Wu. 1995. Use of a stiblenedicarboxamide bridge in stabilizing, monitoring, and photochemically altering folded conformations of oligonucleotides. *J. Am. Chem. Soc*. 117:7323-7328.

97. Lewis, F. D., L. Zhang, R. F. Kelley, D. McCamant, and M. R. Wasielewski. 2007. A perylenedicarboxamide linker for DNA hairpins. *Tetrahedron*. 63:3457-3464.

98. Lewis, F. D., T. Wu, Y. Zhang, R. L. Letsinger, S. R. Greenfield, and M. R. Wasielewski. 1997. Distance-dependent electron transfer in DNA hairpins. *Science*. 277:673-676.

99. Lewis, F. D., Y. Wu, and X. Liu. 2002. Synthesis, structure, and photochemistry of exceptionally stable synthetic DNA hairpins with stilbene diether linkers. *J. Am. Chem. Soc*. 124:12165-12173.

100. Cieplak, P., W. D. Cornell, C. Bayly, P. A. Kollman. 1995. Application of the multimolecule and multiconformational RESP methodology to biopolymers: Charge derivation for DNA, RNA, and proteins. *J. Comput. Chem*. 16:1357-1377.

101. Gaussian 03. Frisch, M. J.; Trucks, G. W.; Schlegel, H. B.; Scuseria, G. E.; Robb, M. A.; Cheeseman, J. R.; Montgomery, Jr., J. A.; Vreven, T.; Kudin, K. N.; Burant, J. C.; Millam, J. M.; Iyengar, S. S.; Tomasi, J.; Barone, V.; Mennucci, B.; Cossi, M.; Scalmani, G.; Rega, N.; Petersson, G. A.; Nakatsuji, H.; Hada, M.; Ehara, M.; Toyota, K.; Fukuda, R.; Hasegawa, J.; Ishida, M.; Nakajima, T.; Honda, Y.; Kitao, O.; Nakai, H.; Klene, M.; Li, X.; Knox, J. E.; Hratchian, H. P.; Cross, J. B.; Bakken, V.; Adamo, C.; Jaramillo, J.; Gomperts, R.; Stratmann, R. E.; Yazyev, O.; Austin, A. J.; Cammi, R.; Pomelli, C.; Ochterski, J. W.; Ayala, P. Y.; Morokuma, K.; Voth, G. A.; Salvador, P.; Dannenberg, J. J.; Zakrzewski, V. G.; Dapprich, S.; Daniels, A. D.; Strain, M. C.; Farkas, O.; Malick, D. K.; Rabuck, A. D.; Raghavachari, K.; Foresman, J. B.; Ortiz, J. V.; Cui, Q.; Baboul, A. G.; Clifford, S.; Cioslowski, J.; Stefanov, B. B.; Liu, G.; Liashenko, A.; Piskorz, P.; Komaromi, I.; Martin, R. L.; Fox, D. J.; Keith, T.; Al-Laham, M. A.; Peng, C. Y.; Nanayakkara, A.; Challacombe, M.; Gill, P. M. W.; Johnson, B.; Chen, W.; Wong, M. W.; Gonzalez, C.; and Pople, J. A.; Gaussian, Inc., Wallingford CT, 2004.

102. Champagne, B. B., J. F. Pfanstiel, D. F. Plusquellic, D. W. Pratt, W. M. Van Herpen, and W. L. Meerts. 1990. Trans-stilbene. A rigid, planar assymetric top in the zero-point vibrational levels of its S0 and S1 electronic states. *J. Phys. Chem*. 94:6-8.

103. Halasinksi, T. M., J. L. Weisman, R. Ruiterkamp, T. J. Lee, F. Salama, and M. Head-Gordon. 2003. Electronic absorption spectra of neutral perylene ($C_{10}H_{12)}$, terrylene ($C_{30}H_{16}$), and quaterrylene ($C_{40}H_{20}$) and their positive and negative ions: Ne matrix-

isolation spectroscopy and time-dependent density functional theory calculations. *J. Phys. Chem.* 107:3660-3669.

104. Sugawa M., Y. Arai, A. H. Iwane, Y. Ishii, and T. Yanagada. 2007. Single-molecule FRET for the study on structural dynamics of biomolecules. *Biosystems*. 88:243-250.

105. Belon, C. A., and D. N. Frick. 2008. Monitoring helicase activity with molecular beacons. *Biotechniques.* 45:433-440.

106. Massey, M., W. R. Algra, U. J. Krull. 2006. Fluorescence resonance energy transfer (FRET) for DNA biosensors: FRET pairs and Förster distances for various dye-DNA conjugates. *Anal. Chem. Acta*. 568:181-189.

107. Widengren, J., and P. Schwille. 2000. Characterization of photoinduced isomerization and back-isomerization of the cyanine dye Cy5 by fluorescence correlation spectroscopy. *J. Phys. Chem. A.* 104:6416-6428.

108. Jia, K., Y. Wan, A. Xia, S. Li, F. Gong, and G. Yang. 2007. Characterization of photoinduced isomerization and intersystem crossing of the cyanind dye Cy3. *J. Phys. Chem. A.* 111:1593-159.

109. Huang, Z., D. Ji, S. Wang, A. Xia, F. Koberling, M. Patting, and R. Erdmann. 2006. Spectral identification of specific photophysics of Cy5 by means of ensemble and single molecule measurements. J. Phys. Chem. A. 110:45-50.

110. Sannborn, M. E., B. K. Connolly, K. Gurunathan, and M. Levitus. 2007. Fluorescence properties and photophysics of the sulfoindocyanine Cy3 linked covalently to DNA. *J. Phys. Chem. B.* 111:11064-11074.

111. Sabanayagam, C. R., J. S. Eid, and A. Meller. 2005. Using fluorescence resonance energy transfer to measure distances along individual DNA molecules: corrections due to nonideal transfer. *J. Chem. Phys*. 122:061103-1-061103-5.

112. Malicka, J., I. Gryczynki, J. Fang, J. Kusba, and J. R. Lakowicz. 2002. Photostability of Cy3 and Cy5-labeled DNA in the presence of metallic silver particles. *J. Fluoresc*. 12:439-447.

113. Shröder G. F., U. Alexiev,and H. Grubmuller. 2005. Simulation of fluorescence anisotropy experiments: Probing protein dynamics. Biophys. J. 89:3757-3770.

114. Mahoney, M. W., and W. L. Joergensen. 2000. Diffusion constant of the TIP5P model of liquid water. J. Chem. Phys. 114:363-366.

115. Sanjit et al. data. (communication)

BIOGRAPHICAL SKETCH

Elena Dolghih was born in Chishinau, Moldova in 1982, where she received her primary and middle school education in Russian. After finishing high school In Limassol, Cyprus in 1998, she moved to Corsicana, Texas to attend Navarro Junior College. She finished her undergraduate studies in 2002 at the University of North Texas with a Bachelor's Degree in Chemistry. She went on to get a Master's degree in Molecular Biology in 2004 under the direction of Dr. Kunz. In 2004, Lena moved to Gainesville, Florida to attend University of Florida and study computational chemistry under the direction of Dr. Krause and, later, Dr. Roitberg.